JCB Journal of Cell Biology

TOOLS

Proteome of the central apparatus of a ciliary axoneme

Lei Zhao, Yuqing Hou, Tyler Picariello, Branch Craige, and George B. Witman

Nearly all motile cilia have a "9+2" axoneme containing a central apparatus (CA), consisting of two central microtubules with projections, that is essential for motility. To date, only 22 proteins are known to be CA components. To identify new candidate CA proteins, we used mass spectrometry to compare axonemes of wild-type *Chlamydomonas* and a CA-less mutant. We identified 44 novel candidate CA proteins, of which 13 are conserved in humans. Five of the latter were studied more closely, and all five localized to the CA; therefore, most of the other candidates are likely to also be CA components. Our results reveal that the CA is far more compositionally complex than previously recognized and provide a greatly expanded knowledge base for studies to understand the architecture of the CA and how it functions. The discovery of the new conserved CA proteins will facilitate genetic screening to identify patients with a form of primary ciliary dyskinesia that has been difficult to diagnose.

Introduction

Nearly all motile cilia and flagella (terms here used interchangeably) contain a "9+2" axoneme consisting of nine outer doublet microtubules and two central microtubules. Periodically arranged along the outer doublet microtubules are a number of substructures, including outer and inner dynein arms, radial spokes, and nexin-dynein regulatory complexes (N-DRCs), that work together to generate and control motility. Genetic and biochemical analyses of these substructures in humans and model organisms, especially *Chlamydomonas reinhardtii*, have resulted in detailed knowledge of their protein composition and function and have revealed a high level of evolutionary conservation of their constituent subunits among motile organisms (Yang et al., 2006; Lin et al., 2011; Bower et al., 2013; King, 2018).

Less well characterized are the central microtubules and their projections, here collectively termed the central apparatus (CA; Loreng and Smith, 2017). The two microtubules of the CA, termed C1 and C2, differ in their stability and projections, which repeat with 16- or 32-nm periodicities along the microtubules. The CA interacts with the radial spokes and has been implicated in the control of ciliary waveform, presumably via the CA → radial spoke → N-DRC → inner dynein arm pathway (Wirschell et al., 2009). It also has a role in the regulation of motility by Ca^{2+}. It is essential for the motility of 9+2 cilia in organisms ranging from *Chlamydomonas* to mammals, and defects in the CA result in infertility, hydrocephalus, and severe respiratory problems in mice and humans (Zhang et al., 2006, 2007; Lechtreck et al., 2008; Olbrich et al., 2012; McKenzie et al., 2015; Edelbusch et al., 2017). Hence, it is imperative to have a detailed knowledge of the CA as well, both to understand how ciliary motility is controlled and to better diagnose human diseases caused by defects in this critical component of the 9+2 axoneme.

In an elegant analysis of *Chlamydomonas* mutants lacking the CA, Adams et al. (1981), using then state-of-the-art 1D and 2D gel electrophoresis, reported that the CA contains 18 different proteins in addition to tubulin. In the decades since then, and in apparently good agreement with the results of Adams et al. (1981), further research on *Chlamydomonas* has resulted in the characterization, at the level of amino-acid sequence, of 22 non-tubulin proteins that are components of the CA. Eighteen of these are unique to the CA, while four appear also to be present elsewhere in the axoneme (Table 1). All have human homologues. Most have been localized to specific projections of either the C1 or C2 microtubule.

Despite the good agreement between the number of CA proteins estimated by 1D and 2D gel electrophoresis and the number that have been characterized at the molecular level, there are reasons to believe that the CA may contain many more proteins that have not yet been identified. First, the 2D gels used for the estimate of Adams et al. (1981) could resolve only ∼250 axonemal proteins, whereas a proteomic analysis of the *Chlamydomonas* flagellum by mass spectrometry (MS) revealed that the axoneme contains approximately twice that many proteins (Pazour et al., 2005), suggesting that the CA also might contain twice as many proteins as previously believed. Second, a recent

Division of Cell Biology and Imaging, Department of Radiology, University of Massachusetts Medical School, Worcester, MA.

Correspondence to George B. Witman: george.witman@umassmed.edu; B. Craige's present address is Department of Biochemistry, Virginia Tech, Blacksburg, VA.

Table 1. **Known CA proteins**

Location	Protein	NCBI accession number	Mass (kD)	References
C1a projection	PF6	AAK38270.1	240	Dutcher et al., 1984; Rupp et al., 2001; Wargo et al., 2005
	FAP101	AAZ31187.1	86	Wargo et al., 2005
	FAP114	AAZ31185.1	32	Wargo et al., 2005
	FAP119	XP_001696622.1	34	Wargo et al., 2005
	FAP227	AAZ31184.1	18	Wargo et al., 2005
	Calmodulin[a]	1206346A	18	Wargo et al., 2005
C1b projection	CPC1	XP_001702926.1	265	Mitchell and Sale, 1999; Zhang and Mitchell, 2004; Mitchell et al., 2005
	FAP42	XP_001697065.1	350	Mitchell et al., 2005
	FAP69	XP_001703508.1	135	Mitchell et al., 2005
	Enolase[a]	XP_001702971.1	56	Mitchell et al., 2005
	HSP70A[a]	XP_001701326.1	78	Mitchell et al., 2005; Shapiro et al., 2005
C1d projection	FAP46	XP_001702776.1	289	DiPetrillo and Smith, 2010
	FAP54	XP_001696950.1	318	DiPetrillo and Smith, 2010
	FAP74	ADD85930.1	204	DiPetrillo and Smith, 2010
	FAP221	ADD85929.2	100	DiPetrillo and Smith, 2010
	FAP297	XP_001690036.1	87	Brown et al., 2012
C1 microtubule	PP1c[a]	AAD38856.1	35	Yang et al., 2000
C2b projection	Hydin	XP_001689997.1	540	Lechtreck and Witman, 2007
C2c projection	KLP1	XP_001701617.1	83	Bernstein et al., 1994; Yokoyama et al., 2004
Others	PF16	XP_001694680.1	57	Dutcher et al., 1984; Smith and Lefebvre, 1996
	PF20	P93107.1	67	Smith and Lefebvre, 1997
	FAP174	ACR55627.1	10	Rao et al., 2016

C1-kinesin (Fox et al., 1994) and AKAP240 (Gaillard et al., 2001) are not listed because their sequences are unknown.
[a]Protein is located both in the CA and elsewhere in the flagellum.

cryo-electron tomography (cryo-ET) analysis of the CA revealed unexpected structural complexity, including four new projections not previously reported (Carbajal-González et al., 2013). Based on this analysis, the C1 microtubule has a total of six projections, termed C1a through C1f, and the C2 microtubule has a total of five projections, termed C2a through C2e. There also is a complex bridge between the two central microtubules, as well as small microtubule inner proteins that are attached to the inside of the C2 microtubule wall. It is difficult to imagine that all of these structures could be built from just 22 proteins. Indeed, the known CA proteins have been localized to just five of the CA projections. Third, the sum of the masses of all the projections as estimated by cryo-ET is >14 MD (Carbajal-González et al., 2013). However, the sum of the masses of all the proteins that have been localized to these projections is just over 3 MD (Table 1). This also suggests that there are many more CA proteins waiting to be discovered.

To search for previously uncharacterized proteins of the CA, we have now compared the proteomes of *Chlamydomonas* WT and CA-less axonemes by label-free quantitative MS. We identified 44 proteins as candidates for being novel CA proteins; at least 13 of these are highly conserved in humans. Detailed studies of five of the conserved proteins confirmed that all five are associated with the CA and cause impaired flagellar motility when missing or defective. Using a combination of genetic, biochemical, and proteomic approaches, we were able to assign many of these proteins to either the C1 or C2 microtubule, and in some cases have been able to predict the specific projections and/or interacting partners with which they are associated. Mutants defective for the confirmed novel CA proteins have a variety of motility phenotypes, indicating different roles for the different proteins. These findings are an important step toward understanding how the CA performs its functions in motile cilia and will facilitate the identification and diagnosis of human patients with defects in the CA.

Results

Selection of *pf18* for comparative MS analysis to identify novel CA proteins

To select the best mutant strain for our studies, we first examined cells of *pf15*, *pf18*, *pf19*, and *pf20*, which partially or totally lack the CA (Adams et al., 1981). As previously reported (Adams et al., 1981), some *pf20* cells had motile flagella, suggesting that some of these cells retained a CA that was at least partially functioning. The flagella of *pf19* were shorter than those of WT,

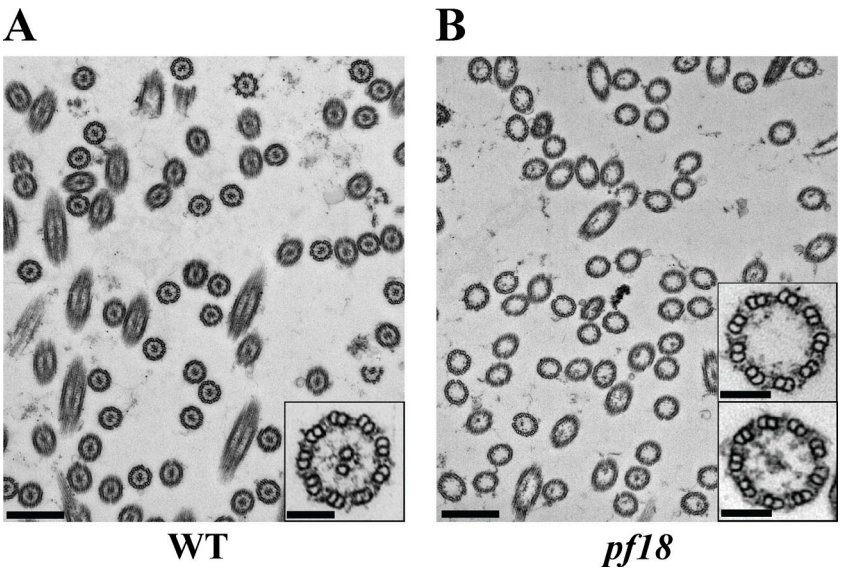

Figure 1. **Structural characterization of WT and *pf18* axonemes used for MS analysis. (A and B)** Representative TEMs of isolated axonemes of WT (A) and *pf18* (B). Nearly all WT axonemes contained a CA, whereas all *pf18* axonemes lacked the CA (see Fig. S1 for quantitation). The axonemes of both preparations were highly pure, with little apparent cell body contamination. Insets: Higher-magnification images confirming integrity of the 9+2 structure in WT axonemes and the 9+0 structure in *pf18* axonemes. The lower inset in B shows that the electron-dense material in the lumens of some *pf18* axonemes is not the CA. Bars, 0.5 µm (A and B); 0.1 µm (insets).

pf15, and *pf18* (Fig. S1 A), raising the possibility that flagellar components other than the CA were defective in this mutant. Thus, strains *pf19* and *pf20* were not considered further. Transmission EM (TEM) of isolated *pf15* and *pf18* axonemes confirmed that all axonemes lacked central microtubules, but revealed that 31% of *pf15* axonemes had electron-dense material (Witman et al., 1978) in the lumens of their axonemes, whereas only 7.5% of *pf18* axonemes had such material (Fig. 1 and Fig. S1, B and C). Except for the absence of the CA, the axonemes of *pf18* appeared structurally normal. Therefore, *pf18* was selected for our comparative proteomics analysis.

Quantitative MS accurately reports abundances of known axonemal proteins in WT and *pf18* axonemes

Preparations of isolated WT and *pf18* axonemes were analyzed by label-free quantitative MS. Both intensity-based absolute quantification (IBAQ; Schwanhäusser et al., 2011) and Top3 precursor quantification (Silva et al., 2006) methods were used to estimate protein abundance; in general, similar results were obtained for the two methods (Table S1). The experiment was repeated twice, generating two independent biological replicates. Data from each replicate (WT vs. *pf18*) were put into a separate dataset. The two datasets together contained a total of 1,364 proteins, of which 75% were detected in both replicates (Table S1). All known proteins of the outer and inner dynein arms, the radial spokes, and the N-DRC were detected in both WT and *pf18* in both replicates, and all known CA proteins were detected in WT in both replicates. Therefore, the datasets are likely to contain most axonemal proteins.

To evaluate our quantitative analysis methods, we first looked at the known axonemal proteins (Fig. 2 A and Table S2). As expected, all outer dynein arm subunits and associated proteins were found in a 1:1 ratio (*pf18*:WT) except for Lis1. That the level of Lis1 is much higher in *pf18* than WT axonemes was previously shown by Western blot analysis and apparently is a cellular response to reduced or disrupted flagellar beating (Rompolas et al., 2012). Similarly, all 25 subunits of the inner dynein arms, all 19 radial spoke subunits for which sequences are available, and all 11 N-DRC subunits were present in a 1:1 ratio (*pf18*:WT).

Both datasets identified 21 of 22 known intraflagellar transport (IFT) particle proteins (IFT43 was not detected). All were significantly elevated in the *pf18* axonemes (Fig. 2 A and Table S2). This is consistent with the previously reported trapping of IFT particles in the axonemal lumen of CA-less mutants (Lechtreck et al., 2013). BBSome proteins and ODA16, which function in IFT (Ahmed et al., 2008; Lechtreck et al., 2009; Hou and Witman, 2017; Taschner et al., 2017), also were greatly increased in *pf18* axonemes; a similar increase for the BBSome protein BBS4 in axonemes of *pf18* and *pf19* was previously shown by Western blotting (Lechtreck et al., 2013).

All 22 of the known CA proteins with reported protein sequences (Table 1) were identified in both datasets (Fig. 2 A and Table S2). As expected, the 18 proteins specific for the CA were greatly decreased in *pf18* (ratio of *pf18*:WT < 0.2). The degree to which each protein was reduced varied, consistent with the observation that residual amounts of some but not other CA proteins could be detected in axonemes of *pf18* and *pf19* by Western blotting (Lechtreck et al., 2013). Protein phosphatase 1 catalytic subunit (PP1c), heat shock protein 70 (HSP70), enolase, and calmodulin, which are located both in the CA and elsewhere in the flagellum (Yang et al., 2000, 2001; Mitchell et al., 2005; Shapiro et al., 2005), were reduced to a lesser extent.

Interestingly, katanin 60/PF19 and katanin 80/PF15, which are required for the assembly of the CA (Dymek et al., 2004; Dymek and Smith, 2012), either were not found or were found at a much lower abundance in WT axonemes than were known CA proteins, and their abundance was not less in *pf18* axonemes (Table S2). This indicates that they are not CA structural proteins, which is consistent with evidence that katanin 80 is located in the basal body region (Esparza et al., 2013). Taken together, the above results show that our approach has identified the vast majority of axonemal proteins

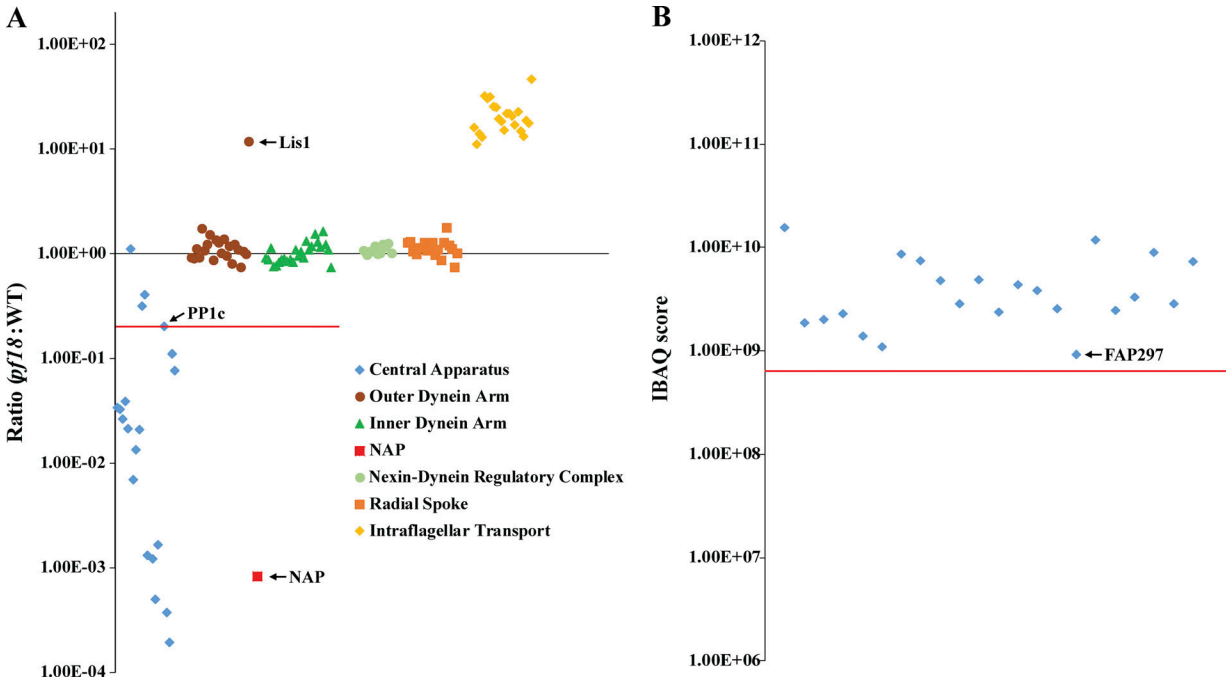

Figure 2. ***pf18*:WT ratios for select flagellar proteins, abundances for known CA proteins, and criteria used to screen for candidate novel CA proteins.** **(A)** *pf18*:WT ratios for axonemal and IFT proteins (in this example, the ratios are based on IBAQ scores from replicate 1; see Table S2). Ratios for subunits such as LC7 and LC8, which are present in more than one axonemal structure, are repeated for each structure with which they are associated. The four CA proteins with the highest ratios (calmodulin, enolase, HSP70, and PP1c, in order of decreasing ratios) are located both in the CA and elsewhere in the flagellum. NAP, an unconventional actin previously shown to be a subunit of some inner arm dyneins in the absence of conventional actin, is grouped separately. Our first criterion for considering an uncharacterized protein as a potentially novel CA component was that it had to have a *pf18*:WT ratio ≤0.2 (red line), ensuring that it is reduced in *pf18* axonemes at least as much as PP1c and the known CA-specific proteins. **(B)** IBAQ values, representing protein abundance, for known CA proteins (values from replicate 1 used as example here). Based on both IBAQ and Top3 values, the least abundant of the known CA proteins in replicate 1 was FAP297. Therefore, our second criterion for considering an uncharacterized protein as a potentially novel CA component was that it had to have an abundance based on IBAQ or Top3 score ≥0.8 of the FAP297 value (red line).

and is accurately reporting their relative amounts in *pf18* versus WT axonemes.

44 novel CA candidate proteins were identified by MS analysis

The quantitative data for the known CA proteins provided a good reference for identifying novel candidate CA proteins. For PP1c, which is predominantly but not exclusively located in the CA (Yang et al., 2000), the *pf18*:WT ratio was 0.2; for all CA-specific proteins, the ratio was <0.2 (Fig. 2 A). Therefore, we screened our datasets for proteins that had *pf18*:WT ratios ≤0.2 (red line in Fig. 2 A). We also needed to set a lower boundary for abundance to eliminate proteins that might be low-level contaminants in the WT preparations but not the *pf18* preparations. Fig. 2 B shows the IBAQ scores, which are a measure of protein abundance, for each of the known CA proteins in the WT axoneme as reported for replicate 1. FAP297, which consistently was the least abundant of these proteins, had an IBAQ score of 9.30×10^8, so we set a boundary at 80% of this value (7.44×10^8) as the lowest IBAQ score that a protein in replicate 1 could have and still be considered a potential candidate CA protein (red line in Fig. 2 B). Proteins in this replicate were similarly screened based on Top3 values and pooled with those selected on the basis of IBAQ scores. Proteins in replicate 2 were screened in the same way using FAP297 abundance values specific to that replicate. From the two replicates, a total of 63 proteins were identified that met both criteria (*pf18*:WT ratio and protein abundance). By definition, these included PP1c and the 18 previously known CA-specific proteins. The remaining 44 proteins (Tables 2 and S3 and Fig. S2) are candidates for being novel CA proteins.

The criteria used to select these 63 proteins were relatively stringent; as a result, Table S1 likely includes additional candidates for novel CA proteins that were excluded from our list of 63 proteins because they fell above our cutoff for *pf18*:WT ratio or below our cutoff for abundance. One such protein may be NAP (novel actin-like protein), an enigmatic protein that replaces conventional actin in some inner arm dyneins when conventional actin is missing (Kato-Minoura et al., 1997) but whose function in the WT cell has been a mystery. Our MS analysis showed that NAP was present in WT axonemes at levels consistently 0.1–0.2 that of FAP297, so it was excluded from our initial list of candidate novel CA proteins. However, it is greatly reduced in *pf18* axonemes (Fig. 2 A), a result that was confirmed by Western blot analysis (Fig. S3 A). Previously, NAP either was not detected in WT axonemes by Western blotting or was detected only in very small amounts (Kato-Minoura et al., 1998; Hirono et al., 2003). Our results suggest that, in the WT axoneme, NAP has some role associated with the CA. Consequently, we have added it to our list of candidate novel CA proteins (Table 2).

Table 2. **Novel candidate CA proteins**

Protein[a]	NCBI accession number	Mass (kD)	Phytozome gene number	Conserved domains	Human homolog[b]	Location
FAP7	XP_001693026.1	55	Cre12.g531800	N	N	?[c]
FAP39	XP_001694877.1	101	Cre02.g145100	Calcium-transporting ATPase	N	C1[d]
FAP47	XP_001691575.1	310	Cre17.g704300	ASH, Calponin homolog	CFAP47	?[c]
FAP49	XP_001696011.1	295	Cre08.g362050	PAS domain	N	C2[c]
FAP65	XP_001702074.1	220	Cre07.g354551[e]	ASH domain	CCDC108	C2[c]
FAP70	XP_001692552.1	114	Cre07.g345400	TPR repeat, VMR2	CFAP70/TTC18	C2[c]
FAP72	XP_001696096.1	595	Cre08.g362000	PAS domain	N	NA
FAP75	XP_001696434.1	125	Cre06.g249900	Adenylate kinase	N	C2[c]
FAP76	XP_001694909.1	162	Cre09.g387689	DUF4455, DUF4456	CCDC180/C9orf174	C1[c]
FAP81	XP_001691318.1	172	Cre06.g296850	ASH domain	DLEC1	C1[c,d]
FAP92	XP_001693652.1	150	Cre13.g562250	N	N	C1[c]
FAP99	XP_001692825.1	90	Cre14.g624400	Neuromodulin family	CFAP99	C1[c]
FAP105	XP_001691070.1	31	Cre12.g511750	N	N	C1[c]
FAP108	XP_001691315.1	22	Cre06.g297200	N	N	C1[c]
FAP123	XP_001703476.1	34	Cre03.g171800	DUF4045 domain	N	?[c]
FAP125	XP_001693959.1	112	Cre12.g546100	Kinesin motor	N	?[c]
FAP139	XP_001694913.1	76	Cre09.g387912	DUF390 domain	N	?[c]
FAP147	XP_001692304.1	97	Cre04.g224250	MYCBP-associated protein family, ASH domain	MYCBP-associated protein	C2[c]
FAP154	XP_001696012.1	467	Cre08.g362100	PAS domain	N	?[c]
FAP171	XP_001692822.1	81	Cre14.g624900	N	N	C2[c]
FAP178	XP_001702799.1	20	Cre10.g418150	Calponin homolog	N	C2[c]
FAP194	XP_001697045.1	52	Cre12.g522150	Armadillo repeat	Spag6	?[c]
FAP216	XP_001702365.1	79	Cre12.g497200	N	N	C1[c]
FAP225	XP_001689770.1	81	Cre01.g051050	EF-hand	N	?[c]
FAP239	XP_001695620.1	23	Cre03.g145387	Mechanosensitive channel	N	C2[c]
FAP246	XP_001689839.1	32	Cre14.g618750	LRR, TGC, EF-hand	LRGUK	C1[c,d]
FAP266[f]	XP_001699180.1	22	Cre16.g690450	MORN repeat	RSP10B	?[c]
	XP_001699181.1					
FAP275	XP_001697713.1	18	Cre05.g239200	N	N	C1[c]
FAP286	XP_001690861.1	17	Cre12.g509800	SMC family	N	C2[c]
FAP289	XP_001700259.1	46	Cre01.g009800	N	N	C1[c]
FAP312	XP_001692669.1	34	Cre14.g630200	Cdk activating kinase	N	C2[c]
FAP345	XP_001701140.1	13	Cre15.g640000	N	N	C1[c]
FAP348	XP_001699354.1	96	Cre16.g693204	N	N	C1[c]
FAP380	XP_001689865.1	20	Cre01.g010400	N	N	?[c]
FAP411	XP_001696779.1	13	Cre09.g409600	N	N	C1[c]
FAP412	XP_001702388.1	57	Cre12.g497450	LRR domain	N	C1[c]
FAP413	XP_001696110.1	37	Cre08.g364000	N	N	C1[c]
FAP414	XP_001694676.1	17	Cre09.g394065	N	N	C1[c]
FAP415	XP_001698357.1	23	Cre10.g454600	N	N	NA
FAP416	XP_001691634.1	17	Cre17.g697750	N	N	NA
FAP417	XP_001702692.1	53	Cre10.g429750	N	N	?[b]
DIP13	XP_001697145.1	13	Cre17.g724550	DUF3552 domain	SSNA1	NA

Table 2. **Novel candidate CA proteins (*Continued*)**

Protein[a]	NCBI accession number	Mass (kD)	Phytozome gene number	Conserved domains	Human homolog[b]	Location
DPY30	XP_001695420.1	11	Cre06.g279100	Dpy-30 domain	Dpy-30	C1[c,d]
MOT17	XP_001697337.1	28	Cre11.g482300	Myosin head family	Spata17	C1[c,d]
NAP[g]	XP_001703266.1	42	Cre03.g176833	Actin superfamily	N	C1[c,d]

N, no conserved domain or no human homolog; NA, data on location incomplete or not reproducible, see "Other" cluster in Fig. 3.
[a]FAP proteins with numbers >410 are given the FAP designation for the first time in this study.
[b]E value ≤10^{-10} and reciprocal best match (except for Spag6, whose reciprocal best match is PF16).
[c]Cluster analysis in Fig. 3.
[d]Coimmunoprecipitation.
[e]The correct Phytozome gene number for FAP65 is Cre07.g354551, but Phytozome has incorrectly associated the name "FAP65" with a different gene.
[f]The sequences corresponding to NCBI XP_001699180.1 and XP_001699181.1 (the former annotated as FAP266) are merged into a single sequence (Cre16.g690450) in Phytozome. Our search identified numerous peptides expressed from both halves of the Phytozome sequence, suggesting that the conjoined model is the correct one for FAP266.
[g]NAP was below the abundance threshold used to identify candidate CA proteins but is included here for reasons discussed in text.

Assignment of candidate novel CA proteins to the C1 or C2 microtubule

We used two approaches to assign the candidate novel CA proteins to either the C1 or C2 microtubule. In the first approach, we took advantage of the fact that the C2 microtubule can be selectively solubilized from isolated axonemes by high-salt treatment, thus leaving most C2-associated proteins in the soluble fraction and most C1-associated proteins in the insoluble fraction (Dutcher et al., 1984; Mitchell and Sale, 1999; Lechtreck and Witman, 2007). We isolated WT axonemes, fractionated them by high-salt treatment and centrifugation, and then analyzed the fractions by quantitative MS to determine the supernatant-to-pellet ratio for each candidate CA protein. A ratio substantially lower than 1 predicts that the protein is a component of the C1 microtubule, whereas a ratio substantially higher than 1 predicts that the protein is a component of the C2 microtubule. In the second approach, we took advantage of the fact that the C1 microtubule is unstable and thus missing from isolated axonemes of the paralyzed flagella mutant *pf16* when the axonemes are demembranated by treatment with detergent in buffer containing 25 mM NaCl (Dutcher et al., 1984; Smith and Lefebvre, 1996; Mitchell and Sale, 1999). We isolated axonemes of WT and *pf16* in this way and then used quantitative MS to estimate the *pf16*:WT ratio for each candidate CA protein. A ratio substantially lower than 1 predicts that the protein is a C1 protein, whereas a ratio of ∼1 predicts that the protein is a C2 protein. The ratios from the two approaches were then used to manually group the known and candidate CA proteins into clusters (Fig. 3 and Table S4).

For the proteins in cluster 1, the soluble:insoluble ratios were <1 and the *pf16*:WT ratios were <1, which means that both approaches predicted that these proteins are associated with the C1 microtubule. Indeed, all 13 known CA proteins in this cluster were previously assigned to C1. Thus, the 18 candidate CA proteins in this cluster are predicted with high confidence to be associated with C1. NAP also is in this cluster and is predicted to be a C1 protein.

Cluster 2 contains hydin, a C2 protein that remains associated with C1 when the C2 microtubule is solubilized (Lechtreck and Witman, 2007). Like hydin, candidate CA proteins FAP47, FAP194, and FAP380 had ratios relatively close to 1 in both experimental approaches, meaning that they are not readily lost from the axoneme when either C1 or C2 is destabilized. They could bridge C1 and C2 directly, or like hydin, they could be part of a projection on one central microtubule and have a stable attachment to a projection on the other central microtubule.

Cluster 3 contains proteins that had soluble:insoluble ratios much greater than 1 and had *pf16*:WT ratios ∼1, meaning that both approaches predicted that these are C2 proteins. Indeed, the two known CA proteins in this cluster previously were assigned to C2. Therefore, the 10 candidate CA proteins in this cluster are predicted with high confidence to be C2 proteins.

The location of the candidate CA proteins in cluster 4 is less certain. These proteins had soluble:insoluble ratios >1 (indicating association with C2) but *pf16*:WT ratios <1 (indicating association with C1). These proteins could be C1 proteins that are extracted from WT axonemes by high salt or C2 proteins that are unstable in *pf16* axonemes. PP1c and FAP297, both previously assigned to C1, are in this cluster. There is evidence that FAP297 is a subunit of the C1d projection of the C1 microtubule (Brown et al., 2012), but it was not identified in an earlier biochemical study of this projection (DiPetrillo and Smith, 2010), suggesting that it may indeed be prone to dissociation from the rest of the projection. In any case, the candidate CA proteins in this cluster cannot be assigned to a specific central microtubule based on these results alone. For proteins in the "other" cluster, the ratios were not reproducible in the biological replicates for one or both approaches (e.g., FAP7 and FAP174), the ratios were different from those of any other protein (FAP225), or the data were incomplete, i.e., the proteins were not detected in one or more of the samples.

Selected candidate CA proteins were confirmed to localize in the CA

To determine how reliable our identification of potentially novel CA proteins was, six of these proteins (DPY30, FAP47, FAP70, FAP76, FAP99, and FAP246) that are highly conserved in humans were selected for further analysis. We also selected two proteins,

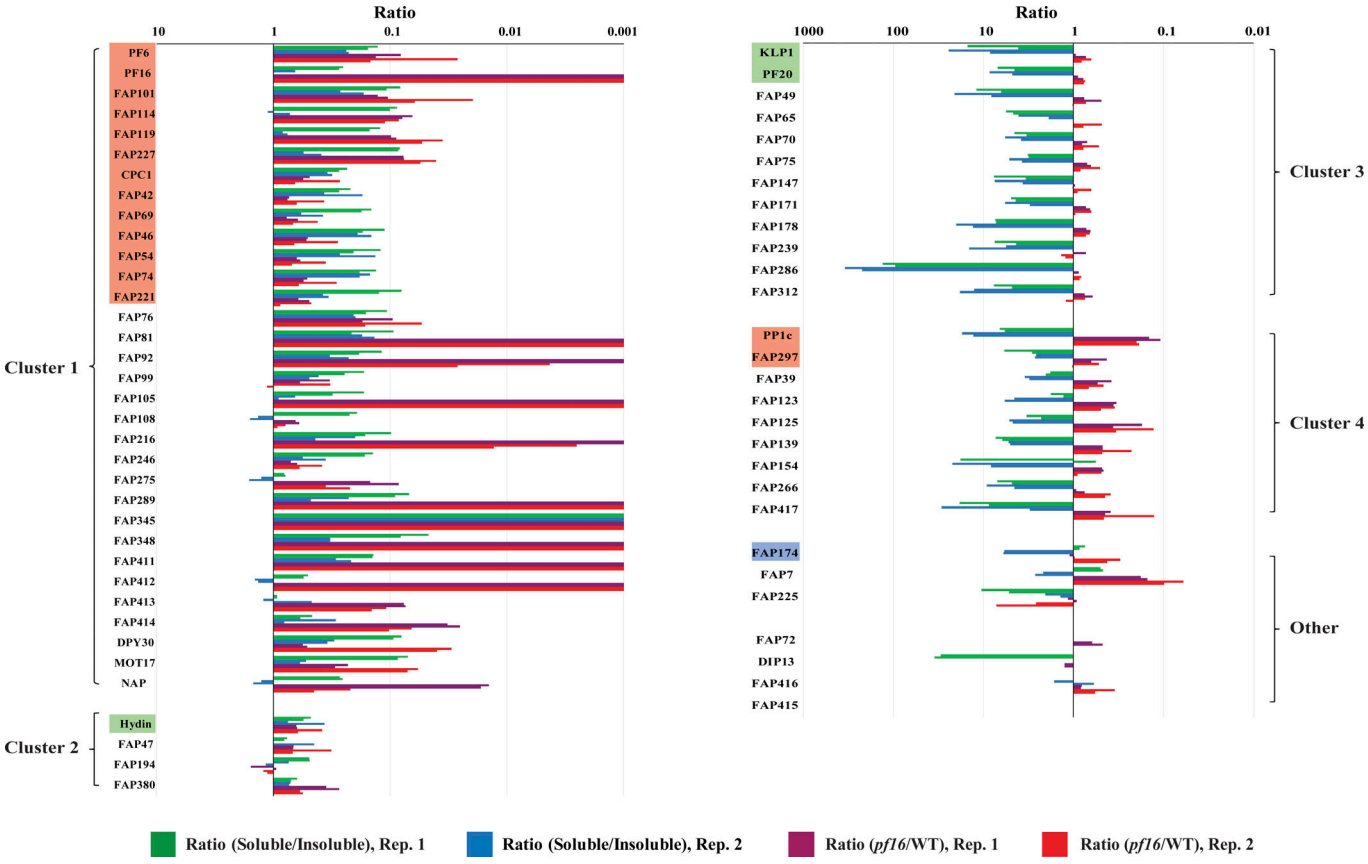

Figure 3. **Assignment of novel candidate CA proteins to the C1 or C2 microtubule.** The results of the two different approaches described in the text were combined to predict association with either the C1 or the C2 microtubule. Each approach was repeated twice to provide two biological replicates (Rep. 1 and Rep. 2), and each replicate was analyzed using IBAQ and Top3 methods. Proteins with similar ratios were then grouped manually into the clusters shown. The soluble:insoluble ratios for replicates 1 and 2 are indicated by green and blue bars, respectively; the *pf16*:WT ratios for replicates 1 and 2 are indicated by purple and red bars, respectively. For each replicate, the ratios as reported by IBAQ and Top3 are shown in that order using the same color. To the left of each bar graph, known C1 proteins are indicated by a light-red background; known C2 proteins have a light-green background. FAP174, indicated by a light-blue background, previously was assigned to C2 (Rao et al., 2016), but this assignment does not fully agree with our other results (see Some candidate proteins can be assigned to specific CA projections). Candidate CA proteins in Cluster 1 are predicted to be C1 proteins, whereas those in Cluster 3 are predicted to be C2 proteins. The locations of candidate CA proteins in the other clusters are less certain.

FAP196 and WNK1, that were greatly reduced in *pf18* axonemes but fell just below our cutoff for abundance. *Chlamydomonas* insertional mutants reported to be defective in the genes encoding these proteins were obtained from the *Chlamydomonas* Library Project (https://www.chlamylibrary.org/; Li et al., 2016). All the mutants were reported to have insertions in the coding regions of the affected genes. We checked the insertion sites by PCR and confirmed the sites for all but *fap70-1* and *wnk1-1*, which were not investigated further (Fig. S4, A–F). The remaining mutants were backcrossed to WT, and progenies containing the insertions (Fig. S4 G) were then transformed with constructs designed to express HA-tagged versions of the WT proteins. Western blot analysis of isolated axonemes from the transformed strains confirmed the presence of these HA-tagged proteins in the axonemes (Fig. S3 B). However, the abundance of FAP196-HA in isolated axonemes was very low; most of the protein was in the cell body (Fig. S3 C). It is possible that the HA tag impeded assembly of FAP196 into the axoneme.

We examined these six mutants for defects in flagella length and swimming speed (Fig. 4, A and B). Among them, *fap76-1* has the shortest flagella and swims the slowest; it also turns more frequently than WT (Fig. 4 C). These *fap76-1* phenotypes were rescued by the HA-tagged FAP76, showing that the insertion in the *FAP76* gene is the underlying cause of the phenotypes. *fap47-1* has flagella that may be slightly longer than normal but swims significantly slower than WT; its slow-swimming phenotype was partially rescued by FAP47-HA. The strain also has a phototaxis defect, which was not rescued by FAP47-HA (Fig. 4 D). However, a second insertional mutant, *fap47-2*, has a similar phototaxis defect (unpublished data), suggesting that FAP47 is important for phototactic steering. Cells of *fap99-1*, *fap246-1*, and *dpy30-1* have normal- or nearly normal-length flagella and swim slightly slower than WT; their slow swimming phenotypes were rescued by the HA-tagged constructs. *fap196-1* had no obvious defects in flagella length or swimming speed.

To determine if these proteins are components of the CA, we used superresolution structured illumination microscopy (SIM) to investigate the locations of the HA-tagged proteins in isolated axonemes. Fig. 5 A shows axonemes from control and FAP47-HA cells probed with anti-HA and anti-acetylated

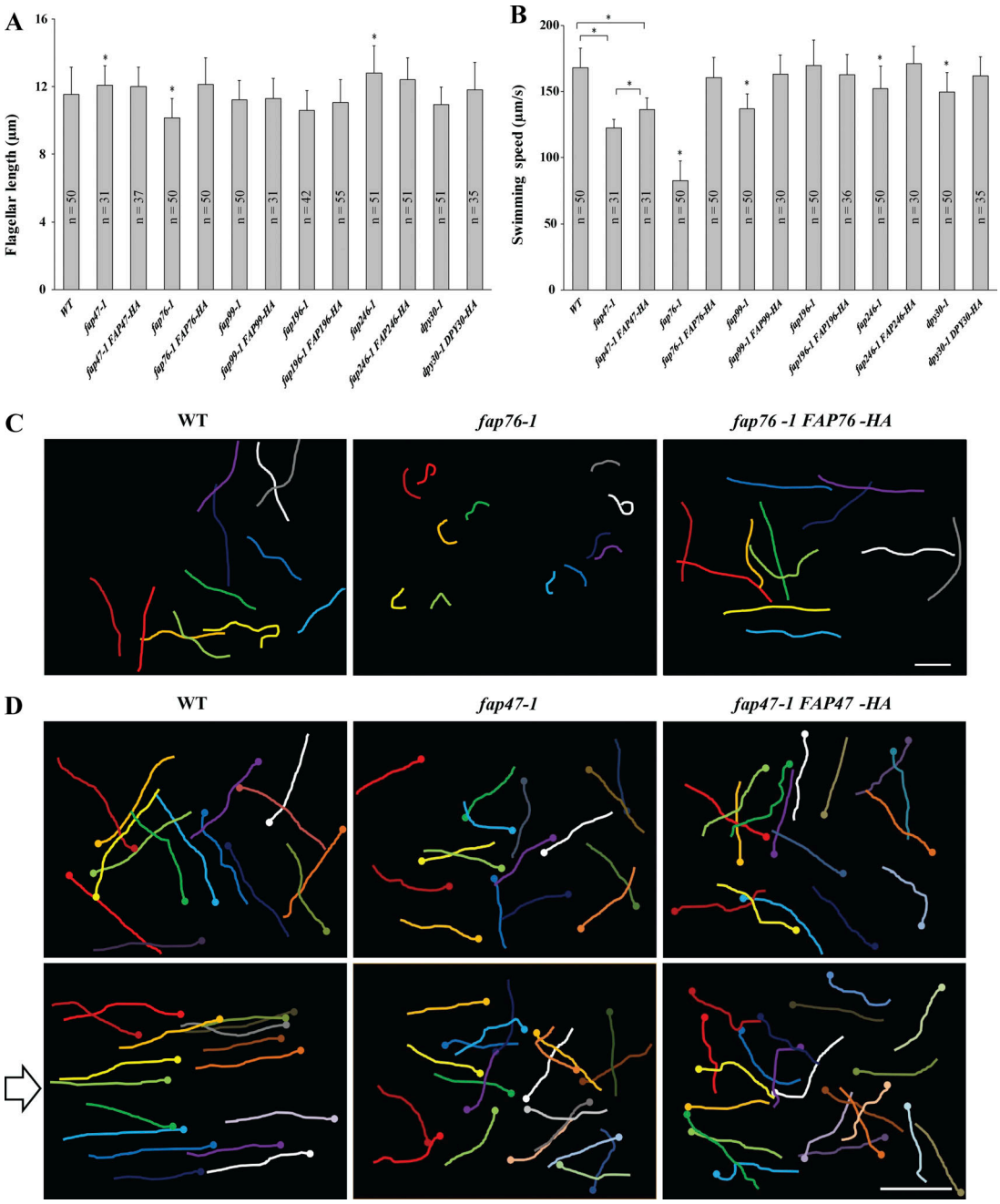

Figure 4. **Phenotypic analysis of insertional mutants and rescued strains. (A)** Flagellar length of WT, the *fap47-1*, *fap76-1*, *fap99-1*, *fap196-1*, *fap246-1*, and *dpy30-1* insertional mutants, and the mutants following transformation with constructs designed to express WT HA-tagged versions of the proteins defective in each. n = number of flagella scored; error bars indicate standard deviation; *, significant difference from WT (Student's *t* test, $P \leq 0.05$). **(B)** Swimming speed of the same strains as in A. n = number of cells scored; error bars indicate standard deviation; *, significant difference (Student's *t* test, $P \leq 0.05$) between WT and mutant or mutant and rescued strains as indicated. **(C)** Swimming paths of WT, the *fap76-1* mutant, and the mutant following transformation with the construct expressing FAP76-HA. The exposure time was 1 s; bar, 50 µm. **(D)** Swimming paths of WT, the *fap*47-1 mutant, and the mutant following transformation with the construct expressing FAP47-HA, in the absence of photostimulation (top panels) and in the presence of photostimulation coming from the left (arrow; lower panels). The large dot in each swimming path indicates the end of the track. *fap47-1* has a slow-swimming phenotype that was partially rescued by FAP47-HA; the phototaxis defect was not noticeably rescued. The exposure time was 0.5 s; bar, 50 µm.

tubulin antibodies. The antibody to the HA tag labels a thin structure that is centered in and runs the entire length of the FAP47-HA axoneme (B, B′, and B″ in Fig. 5 A); no HA signal was detected in control axonemes (i.e., the nonrescued mutants; A, A′, and A″). To confirm that the labeled structure is the CA, the CA was partially (C, C′, and C″ in Fig. 5 A) or completely (D, D′, and D″) extruded from the axoneme by addition of ATP (Mitchell and Nakatsugawa, 2004; Lechtreck and Witman, 2007). In this case, the FAP47-HA signal was clearly associated with the CA but not the rest of the axoneme.

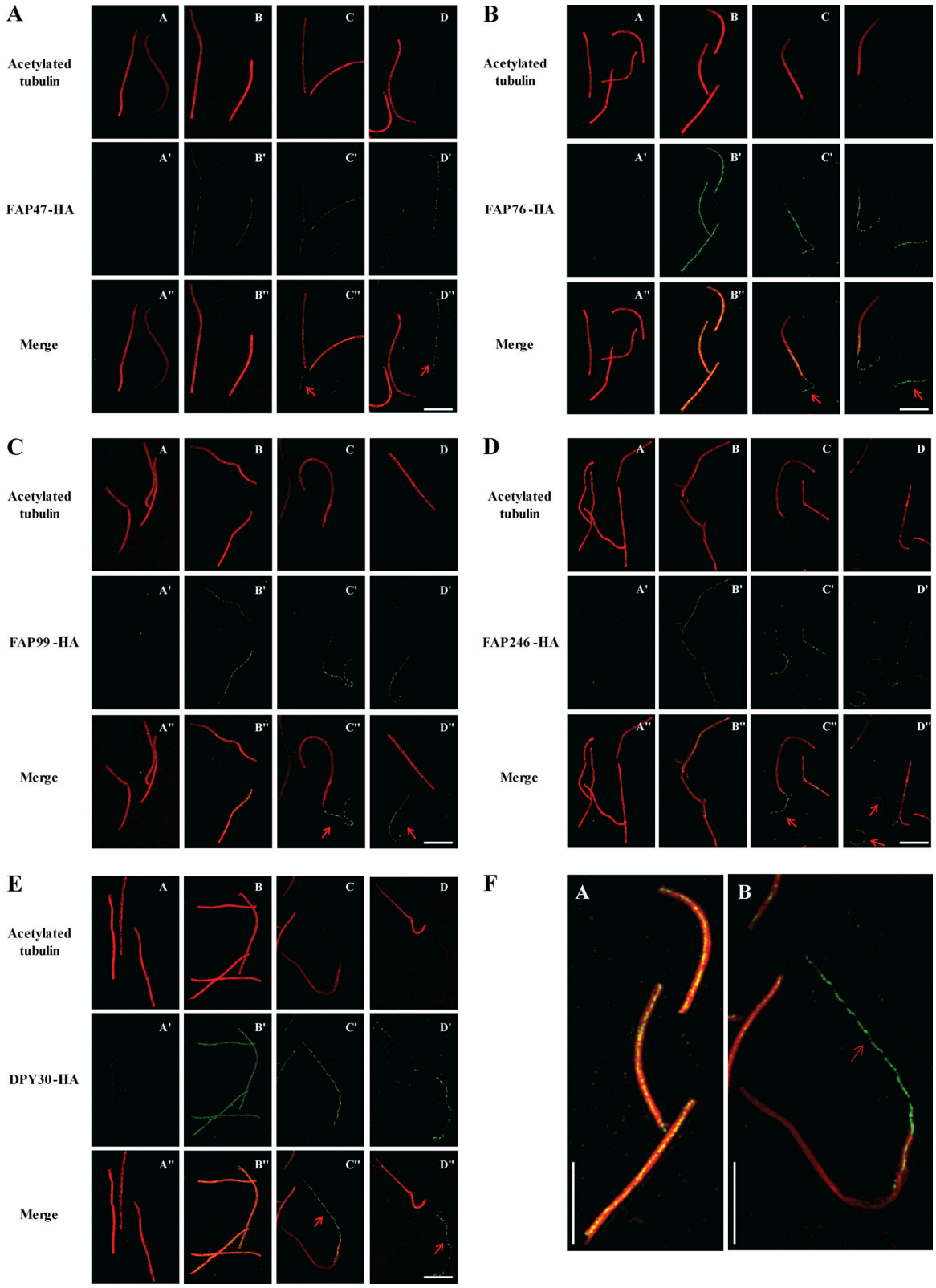

Figure 5. **Localization of selected candidate CA proteins to the CA. (A–E)** SIM images of isolated axonemes from mutant cells rescued with FAP47-HA (A), FAP76-HA (B), FAP99-HA (C), FAP246-HA (D), and DPY30-HA (E). Each set of images shows control intact axonemes from the nonrescued mutant (subpanels A, A′, A″), intact axonemes from the rescued mutant (subpanels B, B′, B″), and axonemes from the rescued mutant after treatment with ATP to induce partial (subpanels C, C′, C″) or complete (subpanels D, D′, D″) extrusion of the CA. Axonemes were double labeled with antibodies to acetylated tubulin (red; A–D) and the HA tag (green; A′–D′); merged images are shown in A″–D″. There was no anti-HA signal from the control axonemes. In the intact rescued axonemes, the CA can be seen as a thin anti-HA–labeled structure centered in and extending the length of the axonemes. In the samples of rescued axonemes with partially or

fully extruded CAs, the CAs appear, respectively, as thin microtubular structures projecting (arrows in C″) or completely separated (arrows in D″) from the axonemes. In the merged images, regions of overlap between the CA and outer doublet microtubules appear yellow. **(F)** (A) Enlargement of B″ from B, and (B) enlargement of C″ from E. Bar, 5 µm.

Therefore, within the axoneme, FAP47 is located exclusively in the CA.

Using the same approach, we determined that FAP76, FAP99, FAP246, and DPY30 also are located exclusively in the CA (Fig. 5, B, C, D, and E, respectively; and see Fig. 5 F for enlargements). No anti-HA signal could be detected in axonemes from FAP196-HA cells (not depicted).

Interacting partners of novel CA proteins and assignment to specific projections of the CA

Having established that the selected candidate CA proteins were indeed components of the CA, we next used immunoprecipitation coupled with MS to identify possible interacting partners for these proteins. Axonemes from WT (control) and the mutant cells rescued with HA-tagged proteins were isolated and extracted with 0.6 M KCl to solubilize most C2 and some C1 microtubules (Pazour et al., 2005). The solubilized HA-tagged proteins were then immunoprecipitated with anti-HA antibodies, and the immunoprecipitates were analyzed by MS. The specificity of coimmunoprecipitation was then assessed on the basis of both abundance relative to the bait protein and enrichment relative to the WT control.

The previously described *fap46-1 FAP46-HA* strain (Brown et al., 2012) was used as a positive control to make sure that our extraction and immunoprecipitation conditions worked for a CA projection. The mutant *fap46-1* is null for FAP46, which is a component of the C1d projection that also contains FAP54, FAP74, FAP221/Pcdp1, and FAP297/C1d-87; *fap46-1* lacks the C1d projection but is completely rescued by FAP46-HA (DiPetrillo and Smith, 2010; Brown et al., 2012). The anti-HA antibody specifically coimmunoprecipitated FAP46-HA and all other known components of C1d with the exception of FAP297 (Table 3 and Table S5). Thus, our conditions appear to be appropriate for investigation of CA protein-interacting partners.

The anti-HA immunoprecipitates from the DPY30-HA strain specifically contained all six of the known C1a proteins (PF6, FAP101, FAP114, FAP119, FAP227, and calmodulin). DPY30-HA and calmodulin were identified by MS in only one of the two biological replicates, probably because they are small proteins (11 and 18 kD, respectively). However, calmodulin is a known component of the C1a projection (Wargo et al., 2005), and Western blotting confirmed that DPY30-HA was present in the sample where MS had failed to detect it (unpublished data). Therefore, DPY30 likely is associated with the C1a projection. In addition, the immunoprecipitate specifically contained two other candidate CA proteins, MOT17 and FAP81, indicating that they also are likely to be novel C1a components. Finally, NAP was specifically and highly enriched in this immunoprecipitate, suggesting that it also is associated with C1a.

The anti-HA immunoprecipitates from the FAP246-HA strain specifically contained the known C1b proteins CPC1, HSP70A, FAP42, and FAP69. In addition, the C1b protein enolase was specifically coimmunoprecipitated in one of the two replicates. Therefore, FAP246 is very likely a C1b protein. The candidate CA proteins FAP39 (101 kD) and FAP174 (10 kD) were specifically enriched in one of the replicates, suggesting, with less confidence, that they also are components of C1b.

The immunoprecipitates from the FAP47-HA, FAP76-HA, and FAP99-HA strains contained the expected HA-tagged protein, but no other proteins were specifically present at similar abundance. It is likely that these HA-tagged proteins were dissociated from their interacting partners by our extraction conditions.

Proteins missing or reduced in axonemes of insertional mutants

To investigate the expression of the novel CA proteins in axonemes of the mutants with defects in the genes encoding these proteins, we used quantitative MS to compare the axonemal proteome of each mutant with that of WT in two biological replicates. In each analysis, we focused on the known and candidate CA proteins that were present in the mutant axonemes in amounts ≤0.2 that of WT (Table 4 and Table S6).

MS of *fap47-1* axonemes detected some FAP47 peptides. In both *fap47-1* samples, all but one of these peptides were encoded by sequence located upstream of the insertion site. The single exception was present in a very low amount compared with the more N-terminal peptides, which themselves were present at a level 0.15–0.27 that in WT. These results indicate that a C-terminally truncated FAP47 is assembled into the *fap47-1* axoneme at a level well below that of full-length FAP47 in the WT axoneme. In addition, candidate CA proteins FAP49, FAP72, FAP154, and FAP416 were greatly reduced in *fap47-1* axonemes, indicating that they are likely to be in the same CA substructure as FAP47 and dependent on FAP47 for their assembly into the axoneme. FAP414 also was substantially reduced, but it was reduced in axonemes of three other mutants as well (see below). Because none of the previously known CA proteins were noticeably affected in this mutant, FAP47 likely is a subunit of a CA substructure that has not previously been characterized biochemically. FAP47 contains ASH (ASPM, SPD-2, Hydin) domains, which may have a role in microtubule binding (Ponting, 2006; Schou et al., 2014); consequently, it is tempting to speculate that FAP47 anchors the complex to the CA via its ASH domains.

Axonemes of the *fap76-1* mutant contained some FAP76 peptides that were encoded only by sequence downstream of the insertion site, indicating that an N-terminally truncated protein is expressed. The abundance (Top3 method) of the truncated protein in the mutant axonemes was much less than that of the full-length protein in WT, suggesting that only a small amount of the truncated protein is assembled into the *fap76-1* axoneme. The only other candidate CA proteins greatly reduced in *fap76-1* axonemes were FAP413, which also was reduced in axonemes from *fap246-1* (see below), and FAP414. As none of the known CA

Table 3. **Proteins identified in immunoprecipitations from axonemal extracts**

Bait	Identified protein	NCBI accession number	Description	Location
FAP46-HA	FAP46	XP_001702776.1	Flagellar associated protein	C1d projection
	FAP54	XP_001696950.1	Flagellar associated protein	C1d projection
	FAP74	ADD85930.1	Flagellar associated protein	C1d projection
	FAP221	ADD85929.2	Flagellar associated protein	C1d projection
FAP47-HA	FAP47	XP_001691575.1	Flagellar associated protein	Unknown
FAP76-HA	FAP76	XP_001694909.1	Flagellar associated protein	C1 microtubule[a]
FAP99-HA	FAP99	XP_001692825.1	Flagellar associated protein	C1 microtubule[a]
FAP246-HA	CPC1	XP_001702926.1	Protein associated with central pair microtubule complex	C1b projection
	FAP42	XP_001697065.1	Adenylate/guanylate kinase-like protein	C1b projection
	FAP69	XP_001703508.1	Flagellar associated protein	C1b projection
	HSP70A	XP_001701326.1	HSP70A	C1b projection
	Enolase[b]	XP_001702971.1	Enolase	C1b projection
	FAP39[b]	XP_001694877.1	Calcium-transporting ATPase	C1b projection
	FAP174[b]	ACR55627.1	Flagellar associated protein	C1b projection
	FAP246	XP_001689839.1	Flagellar associated protein	C1b projection
DPY30-HA	PF6	AAK38270.1	PF6 protein	C1a projection
	FAP101	AAZ31187.1	CA-associated protein C1a-86	C1a projection
	FAP114	AAZ31185.1	CA-associated protein C1a-32	C1a projection
	FAP119	XP_001696622.1	CA-associated protein C1a-34	C1a projection
	FAP227	AAZ31184.1	CA-associated protein C1a-18	C1a projection
	Calmodulin[b]	1206346A	Calmodulin	C1a projection
	DPY30[b]	XP_001695420.1	Subunit of chromatin modifying protein	C1a projection
	FAP81	XP_001691318.1	Flagellar associated protein	C1a projection
	MOT17	XP_001697337.1	Predicted protein	C1a projection
	NAP	XP_001703266.1	Actin-related protein	C1a projection

Previously known CA proteins are indicated by a gray background.
[a]Predicted location based on the cluster analysis of Fig. 3.
[b]Protein was identified or specifically enriched in only one replicate.

proteins were markedly decreased in this mutant, FAP76 also is likely to be a component of a previously uncharacterized CA substructure.

In the two samples of *fap99-1* axonemes, MS detected one and two exclusive unique FAP99 peptides compared with 22 and 20 exclusive unique peptides in the WT samples, indicating that very little of this protein is incorporated into the mutant axoneme. No other candidate or known CA proteins were comparably reduced in these axonemes.

In the two samples of *fap246-1* axonemes, MS detected three and five exclusive unique FAP246 peptides compared with nine exclusive unique peptides in each of the WT samples. IBAQ and Top3 scores for these peptides were much lower in the mutant samples than in WT, suggesting that very little of FAP246 is assembled into the mutant axoneme. FAP413 also was reduced.

No DPY30 peptides were detected in *dpy30-1* axonemes, compared with three and four exclusive unique peptides in the two control samples. No other candidate CA proteins were greatly reduced in the *dpy30-1* axonemes.

FAP196 was readily detected in WT axonemes, but not in *fap196-1* axonemes, indicating that the mutant axoneme is completely devoid of the protein. In addition, FAP414 was considerably reduced.

As noted above, FAP413 was decreased in both *fap76-1* and *fap246-1* axonemes, and FAP414 was decreased in *fap47-1*, *fap76-1*, and *fap196-1* axonemes. These results suggest one of the following possibilities: (a) FAP413 and FAP414 are present in multiple locations in the CA; (b) FAP413 interacts with FAP76 and FAP246, while FAP414 interacts with FAP47, FAP76, and FAP196; or (c) FAP413 and FAP414 associate with the CA nonspecifically.

Discussion

The ensemble of CA proteins is likely to be at least three times greater than previously known

In an effort to identify more CA proteins, we used label-free MS to carry out a comparative proteomics analysis of *Chlamydomonas* WT and CA-less axonemes. The analysis generated a list of 45

Table 4. **Comparative proteomic analysis of WT and mutant axonemes**

Mutant	Protein missing or greatly decreased	Accession number	Description	Predicted location
fap47-1	FAP47[a]	XP_001691575.1	Flagellar associated protein	Unknown
	FAP49	XP_001696011.1	Flagellar associated protein	
	FAP72	XP_001696096.1	Flagellar associated protein	
	FAP154	XP_001696012.1	Flagellar associated protein	
	FAP414[a]	XP_001694676.1	Predicted protein	
	FAP416[a]	XP_001691634.1	Predicted protein	
fap76-1	FAP76	XP_001694909.1	Flagellar associated protein	C1 microtubule[b]
	FAP413	XP_001696110.1	Predicted protein	
	FAP414	XP_001694676.1	Predicted protein	
fap99-1	FAP99	XP_001692825.1	Flagellar associated protein	C1 microtubule[b]
fap196-1	FAP196	XP_001697178.1	Flagellar associated protein	Unknown
	FAP414[c]	XP_001694676.1	Predicted protein	
fap246-1	FAP246	XP_001689839.1	Flagellar associated protein	C1b projection[d]
	FAP413	XP_001696110.1	Predicted protein	
dpy30-1	DPY30	XP_001695420.1	Subunit of chromatin modifying protein	C1a projection[d]

[a]Repeatable in two biological replicates by IBAQ and one replicate by Top3; in the other replicate, Top3 reported that the protein was reduced in the mutant axonemes to only 0.27–0.37 of the WT level. Our cutoff for specificity was that a protein had to be reduced to ≤0.2 of the WT level.
[b]Predicted location based on cluster analysis of Fig. 3.
[c]IBAQ reported that this protein was reduced to <0.2 of the WT level in both biological replicates, whereas Top3 reported that it was present at 0.38 and 2.52 of the WT level in replicates 1 and 2, respectively.
[d]Predicted location based on cluster analysis and supported by coimmunoprecipitation.

candidate novel CA proteins (including NAP), of which at least 13 are conserved in humans (BLAST E ≤ 10^{-10}; Table 2). Further study of five of the conserved proteins by SIM showed that all five are indeed located specifically in the CA, and analysis of these proteins' interacting partners provided evidence that additional candidate proteins are in fact located in the CA. Thus, the total number of CA proteins is likely to be at least three times the number that was previously known.

Assignment of proteins to the C1 or C2 microtubule

By combining data from coimmunoprecipitations and experiments in which either the C1 or C2 microtubule was selectively solubilized, we were able to tentatively assign 20 of the candidate CA proteins to the former and 10 others to the latter (Fig. 6). Eighteen of the previously known CA proteins had been localized to C1, so the total of known and predicted proteins for that microtubule is 38. Only four of the previously known CA proteins were assigned to C2, so the new candidates bring the total for that microtubule to 14 (including FAP174, but see next section). Therefore, the C1 microtubule seems to be associated with about twice as many proteins as the C2 microtubule. This is consistent with the estimate that the total mass of the projections of the C1 microtubule (10.3 MD) is about twice that of the projections of the C2 microtubule (4.3 MD; Carbajal-González et al., 2013).

One of the proteins that we predict is associated with the C2 microtubule is FAP70 (114 kD). Cryo-ET comparison of the outer doublet microtubules of WT *Chlamydomonas* and a *fap70* mutant generated by CRISPR/Cas9 found no structural defect in the mutant doublets, although extra density was detected at the base of the outer dynein arm and on the N-DRC of doublet microtubules from the *fap70* mutant following its rescue with FAP70 fused to the biotin carboxyl carrier protein tag (Shamoto et al., 2018). This led the authors to conclude that FAP70 is located at the base of the outer dynein arm. However, a structural defect or a more definitive localization of the tagged protein might have been observed if the CA had been examined.

Another candidate protein that we predict is associated with the C2 microtubule is FAP49. FAP49, along with FAP47 and three candidate CA proteins (excluding FAP414), was greatly reduced in axonemes of the *fap47-1* mutant, indicating that all five proteins are likely to be part of the same complex (Fig. 6). FAP47 had a solubility profile closely resembling that of hydin, which is located in the C2b projection but remains associated with C1 (and the C1b projection) when C2 is solubilized (Lechtreck and Witman, 2007). The other three proteins could not be clearly assigned to C1 or C2. Thus, it is possible that this complex has connections to both C1 and C2, or to projections emanating from both C1 and C2. Of the five proteins in this complex, three (FAP49, FAP72, and FAP154) are predicted to have PAS (Per-ARNT-Sim) domains. This is remarkable because the entire axoneme contains only six or seven PAS proteins (The Chlamydomonas Flagellar Proteome Project: ChlamyFP; http://chlamyfp.org). Intriguingly, PAS domains in many other proteins are involved in responses to environmental factors such as light, oxygen, and redox potential (Taylor and Zhulin, 1999; Vogt

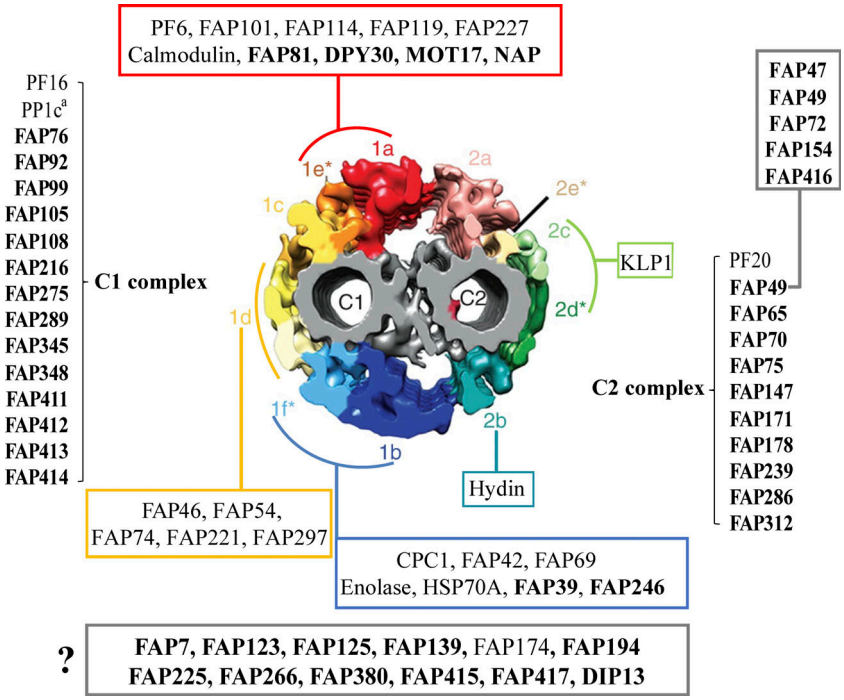

Figure 6. **Summary of CA proteins and their predicted locations in the C1 and C2 microtubules.** Diagram of cross section of the *Chlamydomonas* CA (Carbajal-González et al., 2013) showing predicted locations of previously known CA proteins (normal font) and new candidate or confirmed CA proteins (bold font). Earlier biochemical and structural studies assigned many known proteins to the C1a, C1b, and C2c projections, but more recent cryo-ET data indicate that these structures should be divided into C1a and C1e, C1b and C1f, and C2c and C2d projections, respectively (Carbajal-González et al., 2013). Hence these proteins and new candidate CA proteins that interact with them may be located in either member of these pairs of projections, as indicated by the curved brackets. The FAP47 complex (box, upper right) includes FAP49 and so likely is associated with C2, but where in C2 has not been determined. The question mark indicates proteins whose locations in the CA are not yet known.

and Schippers, 2015). Therefore, it may not be coincidental that the *fap47* mutants appear to have defects in phototaxis.

In the course of these analyses, we also have determined the likely identities of two proteins previously shown to be associated with the CA, but not yet known at the sequence level. One of these, termed C1 kinesin (Loreng and Smith, 2017), had an estimated mass of 110 kD as determined by SDS-PAGE, was recognized by two different anti-peptide polyclonal antibodies generated against conserved kinesin sequences, and was predicted to be a C1 protein (Fox et al., 1994; Mitchell and Sale, 1999). FAP125 is likely to be this kinesin: it has a kinesin motor domain, has a mass of 110,544 D, contains sequences 100% and 70% identical to those used to generate the two pan-kinesin antibodies, and had a *pf16*:WT ratio <1, consistent with it being associated with the C1 microtubule. The second protein, AKAP240, had an estimated mass of 240 kD as determined by SDS-PAGE and was predicted to be associated with the C2 microtubule (Gaillard et al., 2001; Rao et al., 2016). Among our candidate CA proteins, only one matches this description: FAP65 has a predicted mass of 233,007 D and has solubility properties consistent with it being a C2 protein.

Some candidate proteins can be assigned to specific CA projections

When the novel CA protein DPY30-HA was immunoprecipitated, nine other proteins were specifically coimmunoprecipitated, including six previously known CA proteins, two candidate CA proteins (FAP81 and MOT17), and NAP (see next section). The six previously characterized proteins are all known to be subunits of the C1a projection. Therefore, DPY 30 and the other proteins coimmunoprecipitated with it are likely to also be located in the C1a projection, or in an adjacent projection that physically connects to the C1a projection.

Similarly, when the novel protein FAP246 was immunoprecipitated, seven other proteins coimmunoprecipitated with it. Six of these previously had been localized to the CA, and five of them had been localized specifically to the C1b projection. This suggests that FAP246 and the candidate CA protein FAP39, which is one of the proteins coimmunoprecipitated with FAP246, also are components of the C1b projection.

The other protein that was coimmunoprecipitated with FAP246 was FAP174. FAP174 previously was assigned to the C2 microtubule because it was present in demembranated axonemes of *pf16* but was reduced or absent in axonemes of *pf18* and other CA-less mutants (Rao et al., 2016). Our findings that FAP174 is present along with several C1b proteins in FAP246-HA immunoprecipitates suggests that FAP174 is a subunit of either C1b or a projection that interacts with C1b. The C1b and C2b projections physically interact (Mitchell and Sale, 1999; Lechtreck and Witman, 2007; Carbajal-González et al., 2013), and C1b remains associated with the C2 microtubule when the rest of the C1 microtubule is solubilized (Mitchell and Sale, 1999), so a location of FAP174 in either C1b or C2b would be consistent with all evidence to date.

NAP

NAP is a highly divergent member of the actin family that is expressed at very low levels in WT cells but strongly upregulated in the absence of conventional actin (Kato-Minoura et al., 1998; Hirono et al., 2003). Conventional actin is a subunit of several flagellar inner arm dyneins (Piperno and Luck, 1979), and NAP can substitute for actin in some of these dyneins when conventional actin is absent (Kato-Minoura et al., 1997). However, Western blot analysis using an antibody specific for NAP failed to reproducibly detect NAP in axonemes of WT cells, leading to the conclusion that NAP is "present in WT

axonemes in a very small concentration, if present at all" (Kato-Minoura et al., 1998). Further investigation revealed that NAP expression in WT cells is strongly induced by deflagellation, that NAP can be detected in newly formed WT flagella and axonemes by Western blotting, and that the amount of NAP in the axoneme appeared to gradually decrease with time (Hirono et al., 2003), suggesting that NAP may have a role in flagellar assembly.

Our MS analysis of WT axonemes provides compelling evidence that NAP is associated with the axoneme even in the presence of conventional actin. Its 1,000-fold reduction in *pf18* axonemes relative to WT axonemes even though actin levels are unchanged suggests that NAP is uniquely associated with the CA, although it is present in the WT axoneme in an amount ∼100 times less than any previously known CA protein. This very low abundance likely explains why NAP was difficult to reproducibly detect in isolated WT axonemes in the study of Kato-Minoura et al. (1998). Its enrichment along with several known subunits of the C1a projection in immunoprecipitates of DPY30-HA suggests that it may be associated with that projection or with an interacting structure. In support of this, its solubility profile (Fig. 3) is consistent with it being associated with the C1 microtubule. Therefore, we propose that axonemal NAP has some function related to the CA. It may be a structural component of the CA, or it may have a scaffolding function important for CA assembly. Alternatively, NAP may function as an IFT cargo adaptor that links a preassembled CA structure to the anterograde IFT machinery for transport into the flagellum during flagellar assembly, and then largely disappears from the flagellum once assembly is complete. An analogous function recently was reported for IDA3, an IFT cargo adaptor that couples the inner arm dynein I1 to the anterograde IFT machinery (Hunter et al., 2018). It will be of interest to determine if one of the human actin isoforms has a CA association similar to that of NAP.

Mutants with defects in novel CA proteins reveal new roles for CA structures

Previous studies have shown that diverse phenotypes result from defects in specific CA proteins and structures. The *cpc1* mutant, lacking the C1b projection, may be the least affected, with apparently normal forward swimming at a beat frequency that is about two-thirds that of WT and with apparently normal phototactic and photoshock responses (Mitchell and Sale, 1999); the reduced beat frequency may be due to a reduced intraflagellar ATP level as a result of loss of enolase, a subunit of C1b (Mitchell et al., 2005). Other mutations or knockdowns cause more severe phenotypes. The *pf6-2* mutant, which lacks the C1a projection, has flagella that twitch ineffectively so that cells make little or no forward progress (Rupp et al., 2001). Loss of most of projection C2c as a result of RNAi knockdown of the central-pair kinesin Klp1 to ∼20% of its WT level results in a reduction of beat frequency to ∼60% that of WT in most cells, and paralysis in ∼5% of cells (Yokoyama et al., 2004). Loss of the C2b projection as a result of hydin RNAi knockdown causes an unusual form of paralysis in which the flagella of most cells are arrested at the transition points between effective and recovery strokes, indicating a defect in switching dynein arms on and off at specific times during the flagellar beat cycle (Lechtreck and Witman, 2007). Mutations in subunits of the C1d projection cause immotility of most cells and reduced swimming velocity via reduced flagellar beat frequency in those cells that can swim; importantly, phototaxis and photoshock are severely impaired in these mutants, documenting a role for C1d in these behaviors (DiPetrillo and Smith, 2011; Brown et al., 2012). These diverse phenotypes indicate that different CA projections have specific roles, a conclusion that is supported by the unique architecture of each projection (Carbajal-González et al., 2013).

The novel mutants described here expand the range of phenotypes associated with CA defects. Cells of *fap76-1* exhibit a novel CA phenotype in which nearly all cells are motile but swim erratically at about one-half the speed of WT, suggesting impairment of the mechanism controlling cell steering. In another phenotype not previously reported, nearly all *fap47* cells move forward in normal swimming paths at ∼80% the speed of WT and appear to be defective specifically in phototaxis but not photoshock. As mentioned above, this is intriguing because three of the proteins in the FAP47 complex have PAS domains, which have been implicated in transducing environmental signals in many organisms.

Estimated mass of CA projections versus predicted mass of CA proteins

The sum of the masses of the individual CA projections in *Chlamydomonas* as estimated from cryo-ET volume measurements is ∼14.6 MD (Carbajal-González et al., 2013). The total mass of the 22 previously known CA proteins is ∼3.5 MD, and the total mass of the candidate CA proteins identified here is 4.2 MD. Therefore, if all 44 of the latter are indeed CA proteins, the total mass of the identified CA proteins would be 7.7 MD, leaving 6.9 MD still unaccounted for. This "missing" mass would of course be less if some of the proteins are present in multiple copies within a projection. Nevertheless, if there is no systematic error in the mass estimates from cryo-ET, there likely are still many more CA proteins to be identified. Some of the proteins that we found to be greatly reduced in *pf18* axonemes but which did not meet our criteria for inclusion as candidate CA proteins may very well be components of the CA. However, it can be very difficult to precisely estimate masses of large structures by cryo-ET volume measurements, and estimates for the numbers of several subunits in each *Chlamydomonas* N-DRC and radial spoke based on cryo-ET are twice the estimates based on quantitative immunofluorescence and immunoblotting of tagged proteins, suggesting that the volumes/masses were overestimated twofold by cryo-ET (Oda, 2017). If that is also the case for the CA projections, then it is possible that our study has identified nearly all proteins of these structures.

Concluding remarks

Our results reveal that the CA is far more compositionally complex than previously recognized and provide a greatly expanded knowledge base for future studies to understand the architecture of the CA and how it performs its essential functions in motile cilia and flagella. Our results also have significant clinical relevance. In humans, defects in motile cilia cause

primary ciliary dyskinesia (PCD; Horani and Ferkol, 2018). Most known PCD genes affect the nodal cilia, which initiate left–right asymmetry in the early embryo. Errors in this process lead to laterality defects such as situs inversus and heterotaxy in about half of PCD patients; these clinical manifestations, when present, are very helpful for screening potential PCD patients (Shapiro et al., 2018). However, nodal cilia lack a CA, so defects in CA proteins do not cause laterality defects, thus eliminating a key indicator of PCD. Moreover, disruption of individual CA projections is not readily detected by TEM, thus potentially leading to false negatives using that historically important diagnostic tool (Shapiro et al., 2018). As a result, patients who have PCD due to mutations in genes encoding CA components currently are very difficult to diagnose (Edelbusch et al., 2017). Our identification of a large number of novel candidate or confirmed CA proteins that are conserved in humans provides many new potential PCD genes that will be very useful for enhanced genetic screening of patients referred for clinical suspicion of PCD.

Materials and methods

Strains and culture conditions

All *Chlamydomonas* strains used in the work are listed in Table S7. Cells were grown in modified M medium I (Witman, 1986) at 23°C with aeration of 5% CO_2 and a light/dark cycle of 14/10 h.

Flagella preparation and fractionation

Flagella were isolated as described previously (Witman, 1986) and demembranated by resuspension in HMDEK (30 mM Hepes, 5 mM $MgSO_4$, 1 mM DTT, 0.5 mM EGTA, and 25 mM KCl) containing 0.5% NP-40 (Calbiochem) for 10 min at 4°C. The resulting axonemes were collected by centrifugation (30,000 *g* for 20 min) at 4°C. Axonemes prepared in this way were used for the MS analysis of axonemes of WT vs. *pf18*, *fap47-1*, *fap76-1*, *fap99-1*, *fap196-1*, *fap246-1*, and *dyp30-1*. For assignment of CA proteins to the C1 or C2 microtubule, WT axonemes were further extracted with 0.6 M NaCl in HMDEK for 30 min on ice to destabilize the C2 microtubule (Mitchell and Sale, 1999). The sample was then separated into soluble and insoluble fractions by centrifugation, the pellet was resuspended in a volume of HMDEK equal to the volume of the supernatant, and the two fractions were analyzed by MS. To compare *pf16* and WT axonemes, isolated flagella were demembranated in HMDEN (10 mM Hepes, 5 mM $MgSO_4$, 1 mM DTT, 0.5 mM EDTA, 30 mM NaCl, and 0.5% PEG 20,000) with 0.5% NP-40 (Mitchell and Sale, 1999). The axonemes were then collected by centrifugation as above and analyzed by MS.

Genetic crossing

Mutant and WT strains were first spread onto Tris-acetate-phosphate plates (Harris, 1989) and grown for 7–10 d. The cells were then transferred from the plates into a sterile 250-ml flask containing 10 ml of M-N medium (M medium without NH_4NO_3 and with KH_2PO_4 added only to adjust pH to 7.6) and shaken in full light overnight. On the next day, cells were harvested by centrifugation and resuspended in 10 ml of 1/5 M-N medium for 4 h. Aliquots (2–3 ml) of each cell type were then mixed and incubated under light for 2–3 h to allow mating to proceed, after which the mixed cells were collected by centrifugation and resuspended in 1–2 ml of the supernatant. 200–300 µl of the suspension were spread on 4% M medium plates. The plates were dried in the light, sealed with parafilm, left for 3 d in the light, wrapped in foil, left for 10–12 d at room temperature, and then placed at −20°C for 48 h, after which time the cells were allowed to grow on the plates under normal culture conditions. Single colonies were picked for further analysis.

Immunofluorescence and EM

In experiments to determine the locations of select candidate CA proteins, the CA complex was extruded spontaneously from reactivated axonemes as described by Mitchell and Nakatsugawa (2004)with the following modifications: 2.5 µl of 10 mM ATP was added to 18 µl of freshly prepared axonemes to initiate reactivation, and the reactivated axonemes were then incubated at room temperature for 30 min. Then 1.4 µl of 37% formaldehyde (final concentration, 2–3%) was added to fix the samples. For immunofluorescence microscopy, slides were first treated with 0.1% poly-L-lysine (Sigma-Aldrich) for 5–8 min and rinsed with deionized H_2O, and the excess water was wicked off. An aliquot of intact axonemes or axonemes with extruded CAs was then placed on the slide, and the axonemes allowed to adhere for 10 min, after which excess sample was wicked off. The slide was then placed in −20°C methanol for 8–10 min, the excess methanol was wicked off, and the slide was allowed to dry for 20 min at room temperature. The slide was then wetted with 1× PBS for 1 h and flooded with blocking buffer (5% [wt/vol] BSA, 1% [vol/vol] fish skin gelatin, and 10% [vol/vol] goat serum, in 1× PBS) for at least 1 h. The slides were then treated overnight at 4°C with blocking buffer containing the diluted primary antibody (rat anti-HA antibody [Roche; clone 3F10, 1:150]; mouse anti-acetylated tubulin [Sigma-Aldrich; clone 6-11B-1, 1:1,000]). The next day, the slides were washed four times over 1 h with blocking buffer, and then treated for 1 h with blocking buffer containing the secondary antibodies (goat anti-rat IgG [H+L] cross-adsorbed secondary antibody, Alexa Fluor 488 [Invitrogen; A11006, 1:200]; and F(ab′)2-goat anti-mouse IgG [H+L] cross-adsorbed secondary antibody, Alexa Fluor 568 [Invitrogen; A11019, 1:1,000]). The slides were then given two 15-min washes with blocking buffer and transferred to a large volume of 1× PBS for a final wash. After the slides were dried at room temperature, specimens were mounted with ProLong Gold (Invitrogen). SIM was performed using a DeltaVision OMX system (GE Healthcare) with a 1.42 NA 60× Plan-Apochromat objective (Olympus) and immersion oil with a refraction index of 1.512. SIM images were reconstructed with softWoRx 6.1.3 (GE Healthcare). Capture times and adjustments were the same for images with the same antibody. Image brightness and contrast were adjusted using ImageJ (National Institutes of Health). Figures for publication were assembled using Illustrator 8.0 (Adobe).

For TEM, freshly prepared axonemes were fixed in glutaraldehyde and processed as described previously (Hoops and Witman, 1983) with modification. Briefly, the axoneme pellet was fixed at room temperature with 2% glutaraldehyde in

100 mM sodium cacodylate buffer, pH 7.2, for 15 min. The pellet was then teased off from the bottom of the tube, and fixation continued for 1 h. After three 15-min washes with 100 mM sodium cacodylate buffer, the sample was fixed with 1% osmium tetroxide in 75 mM cacodylate buffer at room temperature for 1 h. Next, the pellet was washed twice in 50 mM sodium cacodylate buffer, washed three times in water, and stained en bloc overnight in 1% uranyl acetate at 4°C. On the following day, the sample was given three 10-min washes with water at 4°C, then dehydrated through a graded ethanol series (10%, 30%, 50%, 15 min each; 70%, 85%, 95%, 20 min each; 100%, 30 min), embedded in SPI-Pon 812 Epoxy Resin (SPI), and sectioned at 60–80 nm. Sections were stained with uranyl acetate and lead citrate and viewed with a Phillips CM10 electron microscope.

Gene cloning and vector construction

The hygromycin cassette (Berthold et al., 2002) was first cloned into the HindIII site in pNEB193 (New England Biolabs) to make pBH, and then the vectors were constructed as described immediately below. All the primers used in vector construction are listed in Table S8. Bacterial artificial chromosome (BAC) clones were obtained from Clemson University Genomics Institute (the clones are now available from the Chlamydomonas Resource Center, https://www.chlamycollection.org/).

For the *FAP47* rescue construct, BAC 18J10 containing *FAP47* was digested with BamHI and NheI to obtain 6.9-kb (BamH1-NheI) and 10.7-kb (NheI-NheI) fragments. The 6.9-kb fragment was cloned into pNEB193, yielding pBC1. The 10.7-kb fragment was ligated into pBC1 digested with NheI to yield pBC2. pBC2 was then digested with NdeI and SbfI and ligated into pBH digested with the same enzymes to yield pBC3. To introduce a triple-HA tag, pBC3 was first digested with pfIFI, and the resulting 3.7- and 18.3-kb fragments were purified. The 3.7-kb fragment was ligated into pNEB193 to make pBC4. Sequence encoding the triple-HA tag was amplified with primers F9/R9 from plasmid p3xHA (Silflow et al., 2001) and inserted into pBC4 at the AscI site to yield pBC5. Finally, the 3.7-kb fragment with sequence encoding the triple-HA tag was cut from pBC5 with pfIFI and ligated with the 18.3-kb fragment to yield pBC6.

For the *FAP76* rescue construct, BAC 01H08 was digested with AscI and XbaI to obtain an 8.5-kb fragment containing part of the *FAP76* gene; it was cloned directly into pBH, yielding pBC7. Separately, BAC 01H08 was digested with XbaI to yield a 9.6-kb fragment that contained the rest of the *FAP76* gene. The 9.6-kb fragment was inserted into pBC7 at the XbaI site, yielding pBC8. To introduce a triple-HA tag, sequence encoding the triple-HA tag was amplified from p3xHA with primers F10/R10 and then cloned into pBC8 at the MauB1 site, yielding pBC9.

For the *FAP99* rescue construct, part of *FAP99* was amplified from BAC 32A23 with primers F11/R11 and ligated into pBH between the NdeI and AgeI sites to yield pBC10. A 7.7-kb fragment containing the rest of *FAP99* was cut from BAC 32A23 with AgeI and ligated into pBC10, yielding pBC11. Sequence encoding the triple-HA tag was amplified from the plasmid p3xHA by means of primers F12/R12 and then inserted into pBC11 at the MauB1 site, yielding pBC12.

For the *FAP196* rescue construct, BAC 03D04 containing *FAP196* was digested with AscI and SbfI to obtain 5.6-kb (AscI-SbfI) and 9.1-kb (SbfI-SbfI) fragments. The 5.6-kb fragment was cloned into pBH between the AscI and the SbfI sites, yielding pBC13. The 9.1-kb fragment was ligated into pBC13 at the SbfI site, yielding pBC14. To introduce a triple-HA tag, pBC14 was first digested with MauB1 and BglII to yield 2.8- and 16.3-kb fragments. The 2.8-kb fragment was ligated into pNEB193 to make pBC15. Sequence encoding the triple-HA tag was amplified from the plasmid p3xHA by means of primers F13/R13 and inserted into pBC15 at the PfoI site, yielding pBC16. Then, the 2.8-kb fragment tagged with sequence encoding 3HA was cut from pBC16 with MauB1 and BglII and ligated with the 16.3-kb fragment, yielding pBC17.

For the *FAP246* rescue construct, a 10.2-kb fragment containing part of the *FAP246* gene was cut from BAC 38L21 with AgeI and NheI and ligated into pBH, yielding pBC18. The rest of the *FAP246* gene was then amplified from BAC 38L21 with primers F14/R14 and ligated into pBC18 between its PacI and AgeI sites to yield pBC19. To insert a sequence encoding the triple-HA tag into the gene, part of *FAP246* was amplified from BAC clone 38L21 using primers F15/R15; the resulting fragment was ligated into pNEB193 at the BamHI and HindIII sites to yield pBC20. Sequence encoding the triple-HA tag was amplified from the plasmid p3xHA by means of primers F16/R16 and cloned into pBC20 at the SacII site, yielding pBC21. Then the partial *FAP246* gene with 3xHA-encoding sequence was cut from pBC21 with PasI and SfiI and used to replace its untagged counterpart in pBC19 to yield pBC22.

For the *DPY30* rescue construct, *DPY30* was amplified from BAC 23P20 with primers F17/R17 and cloned into pBH with XmaI and PacI, yielding pBC23. To introduce a triple-HA tag, sequence encoding the triple-HA tag was amplified from the plasmid p3xHA by means of primers F18/R18 and then cloned into pBC23 with AscI, yielding pBC24.

All constructs were verified by sequencing. DNA transformation was done by the glass bead method (Kindle, 1990). After transformation, cells were grown on Tris-acetate-phosphate agar supplemented with 10 µg/ml hygromycin (Sigma-Aldrich). Colonies derived from single cells were picked and screened for incorporation of the rescuing construct by PCR with primers listed in Table S8. Incorporation of the construct was confirmed by Western blotting before phenotypic analysis.

Immunoprecipitation and identification of interacting partners

For immunoprecipitation with the anti-HA peptide antibody, axonemes isolated as above were resuspended in high-salt buffer (30 mM Hepes, pH 7.4, 5 mM $MgSO_4$, 1 mM DTT, 0.5 mM EGTA, and 0.6 M KCl) and incubated on ice for 30 min to solubilize most C2 microtubules and some C1 microtubules (Pazour et al., 2005). The suspension was then centrifuged (30,000 *g* for 20 min at 4°C), and the supernatant was collected as the KCl extract. 50 µl of anti-HA Affinity Matrix (Roche) and Mini Protease Inhibitor Cocktail (Roche; 11836170001) was mixed with the KCl extract (77 µg of total protein), and the mixture was incubated with rotation overnight at 4°C. After four washes with high-salt buffer, bound proteins were eluted for

20 min at room temperature with 80 µl of 1 mg/ml HA peptide in 167 mM NaCl, 10 mM Tris-HCl, pH 7.5, 0.05% Tween 20, and 0.25× Mini Protease Inhibitor Cocktail. Western blotting was used to confirm that the tagged protein was eluted from the matrix. Immunoprecipitates were then analyzed by MS, and protein abundance was estimated with both IBAQ or Top3 quantification methods. Experiments for DPY30 and FAP246 were repeated twice to generate two biological replicates.

Only previously known or newly identified candidate CA proteins were considered as potential interacting partners in each immunoprecipitation. In general, to be designated a specifically interacting partner, a protein had to have an abundance in the experimental immunoprecipitate ≥1/10 that of the bait protein and had to be enriched in the experimental immunoprecipitate ≥10-fold relative to the same protein in the WT control immunoprecipitate, based on either IBAQ or Top3 scores. For those cases in which previously known subunits of a CA projection were identified in the experimental immunoprecipitate, a protein was considered specifically interacting (a) if its abundance in the experimental immunoprecipitate was greater than that of the least abundant subunit from the projection, and (b) if it was enriched in the experimental immunoprecipitate at least as much as the least enriched of the previously known subunits, or enriched ≥10-fold, whichever was larger. In the cases of DPY30 and FAP246, if a protein from either replicate met these criteria, it was designated an interacting partner.

Western blotting

Protein samples were subjected to SDS-PAGE using 4–20% precast gels (Bio-Rad). Western blots were prepared by transferring proteins from gels to polyvinylidene difluoride membrane (Immobilon P; Millipore). The Western blots were probed with rat monoclonal anti-HA antibody (Roche; clone 3F10) at 1:1,000 dilution or rabbit polyclonal anti-NAP antibody (Kato-Minoura et al., 1998; kindly provided by Dr. S. King, University of Connecticut Health Center, Farmington, CT) at 1:2,000 dilution. For detection of loading controls, blots were probed with mouse monoclonal antibody to outer arm dynein intermediate chain IC2 (King et al., 1985) at 1:250 dilution or mouse monoclonal antibody to α-tubulin (Sigma-Aldrich; clone B-5-1-2) at 1:1,000 dilution.

Motility analysis, photobehavioral assays, and flagellar length measurement

All observations and recordings were performed at room temperature. To analyze swimming speed, 50 µl of cell culture were transferred to a plastic chamber (0.127-mm-deep Fisherbrand UriSystem DeciSlide; Thermo Fisher Scientific). Cells were imaged with nonactinic (deep-red) light using a Zeiss inverted microscope equipped with a 16×/0.35 NA Plan objective and a Kopp #2408 red long-pass filter (Kopp Glass). Videos were recorded at 30 images/s with a digital charge-coupled camera (UP-610; UNIQ Vision) and Video Savant 3.0 software (IO Industries). Swimming speeds were determined using ImageJ software as previously described (Awata et al., 2015). To assess phototactic behavior, cells in 0.8-mm-deep chambers constructed of two coverslips were illuminated from one side with a stimulus beam of light as previously described (Moss et al., 1995) and recorded using the above microscope, camera, and software. Photoshock was visually assayed by viewing swimming cells with red light using a Zeiss Universal microscope equipped with a NEOFLUAR 16×/0.40 Ph2 objective, and then quickly removing the red filter. For video microscopy of photoshock, swimming cells illuminated by nonactinic red light, in the same setup as for assay of phototaxis, were suddenly exposed to a stimulus beam of white light coming from the side. To record swimming tracks, 1-s exposures were acquired using white light and phase-contrast optics on a Zeiss Axioskop 2 Plus microscope equipped with a 20× Plan-NEOFLUAR 0.5 NA Ph2 objective, a digital charge-coupled camera (AxioCam MRm), and AxioVision 3.1 software (Zeiss).

For flagellar length measurement, cells were fixed in 2% glutaraldehyde and then imaged using phase-contrast optics and the Axioskop 2 Plus microscope equipped with a 40× Plan-NEOFLUAR 0.75 NA Ph2 objective. Images were recorded using AxioVision software, and flagellar lengths were then determined with ImageJ.

MS

For comparison of WT and mutant axonemes, axonemes were isolated as above, and protein concentration was determined using a Bradford Protein Assay Kit (Thermo Fisher Scientific; 23200). Equivalent amounts of WT and mutant axonemal protein were fully resolved by 1D 4–20% gradient SDS-PAGE, and each lane was then cut into five segments, such that each segment had an approximately equal amount of protein. Each segment was then processed separately. For analysis of soluble and insoluble fractions generated by extraction of WT axonemes with 0.6 M NaCl, the samples were treated similarly except that the gel lanes were loaded with equal volumes of the samples, and each lane was cut into four segments. For analysis of immunoprecipitates, proteins in control and experimental samples were electrophoresed a short distance into an SDS-polyacrylamide gel and the segments containing the unresolved proteins then excised.

In-gel digestion and liquid chromatography–MS/MS analysis were performed in the Mass Spectrometry Facility of University of Massachusetts Medical School as described before (Kubo et al., 2018) with modification. Briefly, the gel segments were treated with trypsin and then subjected to reduction with DTT and alkylation with iodoacetamide. Peptides eluted from the gel were lyophilized and resuspended in 25 µl of 5% acetonitrile (0.1% [vol/vol] TFA). 3 µl of each sample, in technical singlicate, were loaded by a Waters NanoAcquity UPLC in 5% acetonitrile (0.1% formic acid) at 4.0 µl/min for 4.0 min onto a 100-µm-internal-diameter (ID) fused-silica precolumn packed with 2 cm of 5 µm (200 Å) Magic C18AQ (Bruker-Michrom). Peptides were eluted at 300 nl/min from a 75-µm-ID gravity-pulled analytical column packed with 25 cm of 3-µm (100 Å) Magic C18AQ particles using a linear gradient from 5 to 35% of mobile phase B (acetonitrile + 0.1% formic acid) in mobile phase A (water + 0.1% formic acid) over 60 min. Ions were introduced by positive electrospray ionization via liquid junction at 1.5 kV into a

Thermo Fisher Scientific Q Exactive hybrid mass spectrometer. Mass spectra were acquired over *m/z* 300–1,750 at 70,000 resolution (*m/z* 200) with an AGC target of 1e6, and data-dependent acquisition selected the top 10 most abundant precursor ions for tandem MS by HCD fragmentation using an isolation width of 1.6 D, maximum fill time of 110 ms, and AGC target of 1e5. Peptides were fragmented by a normalized collisional energy of 27, and fragment spectra acquired at a resolution of 17,500 (*m/z* 200).

Data analysis

Raw data files were peak processed with Proteome Discoverer (version 2.1; Thermo Fisher Scientific) followed by identification using Mascot Server (version 2.5 or 2.6; Matrix Science) against the National Center for Biotechnology Information (NCBI) protein databases. Search parameters included Trypsin/P specificity, up to two missed cleavages, a fixed modification of carbamidomethyl cysteine, and variable modifications of oxidized methionine, pyroglutamic acid for Q, and N-terminal acetylation. Assignments were made using a 10-ppm mass tolerance for the precursor and 0.05-D mass tolerance for the fragments. All nonfiltered search results were loaded into Scaffold (version 4.8; Proteome Software), with gel fractions loaded as technical replicates and further processed by Scaffold using the Trans-Proteomic Pipeline (Institute for Systems Biology) with all peptides filtered to a 1% false discovery rate. Only proteins identified by two or more peptides, with a protein threshold of 90% probability and a peptide threshold of 90% probability, were considered "detected" and were included in the subsequent analysis. IBAQ (Schwanhäusser et al., 2011) and Top3 precursor quantification methods (Silva et al., 2006) were used to estimate the abundance of each protein.

Domain predictions

ASH domains were confirmed using the NCBI Conserved Domain tool (https://www.ncbi.nlm.nih.gov/Structure/cdd/wrpsb.cgi; threshold, 100). PAS domains were confirmed by searching proteins on the SMART website (http://smart.embl-heidelberg.de/).

Online supplemental material

Fig. S1 shows the flagellar length and ultrastructure of axonemes of WT and *pf* mutants. Fig. S2 shows the Venn diagram of known and candidate CA proteins in replicates 1 and 2. Fig. S3 shows that NAP is present in WT axonemes and absent from *pf18* axonemes, and that HA-tagged proteins are expressed in the axonemes of the rescued strains as confirmed by Western blots. Fig. S4 shows confirmation of mutant insertion sites by PCR. Table S1 lists all the proteins quantified in two independent biological replicates comparing WT and *pf18* axonemes. Table S2 contains the MS data for the proteins in Fig. 2. Table S3 contains the MS data for the candidate CA proteins. Table S4 contains the MS data for Fig. 3. Table S5 contains the MS data for the immunoprecipitation experiments of Table 3. Table S6 contains the MS data for the comparative proteomics experiments of Table 4. Tables S7 and S8 list the strains and primers used in this study, respectively.

Acknowledgments

We are grateful to Dr. S. King for his generous gift of anti-NAP antibody. From the University of Massachusetts Medical School, we thank Dr. G. Pazour and Mr. N. McNeill for help with protein analysis; Ms. D. Cochran for technical assistance; Drs. G. Hendricks and L. Strittmatter and Mr. K. Reddig of the Electron Microscopy Facility for expert assistance with EM; Drs. J. Leszyk and M. Dubuke at the Mass Spectrometry Facility for expert assistance with MS; and Dr. C. Baer of the Sanderson Center for Optical Experimentation (SCOPE) Imaging Facility for expert assistance with SIM.

This work was supported by National Institutes of Health grants R37 GM030626 and R35 GM122574 to G.B. Witman and by the Robert W. Booth Endowment at the University of Massachusetts Medical School to G.B. Witman.

The authors declare no competing financial interests.

Author contributions: L. Zhao, Y. Hou, and G.B. Witman conceived the project and designed the experiments. L. Zhao performed most of the experiments and data analysis. Y. Hou performed the MS analysis of insertional mutants. T. Picariello and B. Craige contributed advice and reagents for the genetic crossing, vector construction, and immunofluorescence microscopy. L. Zhao, Y. Hou, and G.B. Witman wrote the manuscript.

Submitted: 3 February 2019
Revised: 13 April 2019
Accepted: 17 April 2019

References

Adams, G.M., B. Huang, G. Piperno, and D.J. Luck. 1981. Central-pair microtubular complex of Chlamydomonas flagella: polypeptide composition as revealed by analysis of mutants. *J. Cell Biol.* 91:69–76. https://doi.org/10.1083/jcb.91.1.69

Ahmed, N.T., C. Gao, B.F. Lucker, D.G. Cole, and D.R. Mitchell. 2008. ODA16 aids axonemal outer row dynein assembly through an interaction with the intraflagellar transport machinery. *J. Cell Biol.* 183:313–322. https://doi.org/10.1083/jcb.200802025

Awata, J., K. Song, J. Lin, S.M. King, M.J. Sanderson, D. Nicastro, and G.B. Witman. 2015. DRC3 connects the N-DRC to dynein g to regulate flagellar waveform. *Mol. Biol. Cell.* 26:2788–2800. https://doi.org/10.1091/mbc.E15-01-0018

Bernstein, M., P.L. Beech, S.G. Katz, and J.L. Rosenbaum. 1994. A new kinesin-like protein (Klp1) localized to a single microtubule of the Chlamydomonas flagellum. *J. Cell Biol.* 125:1313–1326. https://doi.org/10.1083/jcb.125.6.1313

Berthold, P., R. Schmitt, and W. Mages. 2002. An engineered Streptomyces hygroscopicus aph 7" gene mediates dominant resistance against hygromycin B in Chlamydomonas reinhardtii. *Protist.* 153:401–412. https://doi.org/10.1078/14344610260450136

Bower, R., D. Tritschler, K. Vanderwaal, C.A. Perrone, J. Mueller, L. Fox, W.S. Sale, and M.E. Porter. 2013. The N-DRC forms a conserved biochemical complex that maintains outer doublet alignment and limits microtubule sliding in motile axonemes. *Mol. Biol. Cell.* 24:1134–1152. https://doi.org/10.1091/mbc.e12-11-0801

Brown, J.M., C.G. Dipetrillo, E.F. Smith, and G.B. Witman. 2012. A FAP46 mutant provides new insights into the function and assembly of the C1d complex of the ciliary central apparatus. *J. Cell Sci.* 125:3904–3913. https://doi.org/10.1242/jcs.107151

Carbajal-González, B.I., T. Heuser, X. Fu, J. Lin, B.W. Smith, D.R. Mitchell, and D. Nicastro. 2013. Conserved structural motifs in the central pair complex of eukaryotic flagella. *Cytoskeleton (Hoboken).* 70:101–120. https://doi.org/10.1002/cm.21094

DiPetrillo, C.G., and E.F. Smith. 2010. Pcdp1 is a central apparatus protein that binds Ca(2+)-calmodulin and regulates ciliary motility. *J. Cell Biol.* 189:601–612. https://doi.org/10.1083/jcb.200912009

DiPetrillo, C.G., and E.F. Smith. 2011. The Pcdp1 complex coordinates the activity of dynein isoforms to produce wild-type ciliary motility. *Mol. Biol. Cell.* 22:4527–4538. https://doi.org/10.1091/mbc.e11-08-0739

Dutcher, S.K., B. Huang, and D.J. Luck. 1984. Genetic dissection of the central pair microtubules of the flagella of Chlamydomonas reinhardtii. *J. Cell Biol.* 98:229–236. https://doi.org/10.1083/jcb.98.1.229

Dymek, E.E., and E.F. Smith. 2012. PF19 encodes the p60 catalytic subunit of katanin and is required for assembly of the flagellar central apparatus in Chlamydomonas. *J. Cell Sci.* 125:3357–3366. https://doi.org/10.1242/jcs.096941

Dymek, E.E., P.A. Lefebvre, and E.F. Smith. 2004. PF15p is the chlamydomonas homologue of the Katanin p80 subunit and is required for assembly of flagellar central microtubules. *Eukaryot. Cell.* 3:870–879. https://doi.org/10.1128/EC.3.4.870-879.2004

Edelbusch, C., S. Cindrić, G.W. Dougherty, N.T. Loges, H. Olbrich, J. Rivlin, J. Wallmeier, P. Pennekamp, I. Amirav, and H. Omran. 2017. Mutation of serine/threonine protein kinase 36 (STK36) causes primary ciliary dyskinesia with a central pair defect. *Hum. Mutat.* 38:964–969. https://doi.org/10.1002/humu.23261

Esparza, J.M., E. O'Toole, L. Li, T.H. Giddings Jr., B. Kozak, A.J. Albee, and S.K. Dutcher. 2013. Katanin localization requires triplet microtubules in Chlamydomonas reinhardtii. *PLoS One.* 8:e53940. https://doi.org/10.1371/journal.pone.0053940

Fox, L.A., K.E. Sawin, and W.S. Sale. 1994. Kinesin-related proteins in eukaryotic flagella. *J. Cell Sci.* 107:1545–1550.

Gaillard, A.R., D.R. Diener, J.L. Rosenbaum, and W.S. Sale. 2001. Flagellar radial spoke protein 3 is an A-kinase anchoring protein (AKAP). *J. Cell Biol.* 153:443–448. https://doi.org/10.1083/jcb.153.2.443

Harris, E.H. 1989. *The* Chlamydomonas *Sourcebook.* Academic Press, San Diego. 780 pp.

Hirono, M., S. Uryu, A. Ohara, T. Kato-Minoura, and R. Kamiya. 2003. Expression of conventional and unconventional actins in Chlamydomonas reinhardtii upon deflagellation and sexual adhesion. *Eukaryot. Cell.* 2:486–493. https://doi.org/10.1128/EC.2.3.486-493.2003

Hoops, H.J., and G.B. Witman. 1983. Outer doublet heterogeneity reveals structural polarity related to beat direction in Chlamydomonas flagella. *J. Cell Biol.* 97:902–908. https://doi.org/10.1083/jcb.97.3.902

Horani, A., and T.W. Ferkol. 2018. Advances in the Genetics of Primary Ciliary Dyskinesia: Clinical Implications. *Chest.* 154:645–652. https://doi.org/10.1016/j.chest.2018.05.007

Hou, Y., and G.B. Witman. 2017. The N-terminus of IFT46 mediates intraflagellar transport of outer arm dynein and its cargo-adaptor ODA16. *Mol. Biol. Cell.* 28:2420–2433. https://doi.org/10.1091/mbc.e17-03-0172

Hunter, E.L., K. Lechtreck, G. Fu, J. Hwang, H. Lin, A. Gokhale, L.M. Alford, B. Lewis, R. Yamamoto, R. Kamiya, et al. 2018. The IDA3 adapter, required for intraflagellar transport of I1 dynein, is regulated by ciliary length. *Mol. Biol. Cell.* 29:886–896. https://doi.org/10.1091/mbc.E17-12-0729

Kato-Minoura, T., M. Hirono, and R. Kamiya. 1997. Chlamydomonas inner-arm dynein mutant, ida5, has a mutation in an actin-encoding gene. *J. Cell Biol.* 137:649–656. https://doi.org/10.1083/jcb.137.3.649

Kato-Minoura, T., S. Uryu, M. Hirono, and R. Kamiya. 1998. Highly divergent actin expressed in a Chlamydomonas mutant lacking the conventional actin gene. *Biochem. Biophys. Res. Commun.* 251:71–76. https://doi.org/10.1006/bbrc.1998.9373

Kindle, K.L. 1990. High-frequency nuclear transformation of Chlamydomonas reinhardtii. *Proc. Natl. Acad. Sci. USA.* 87:1228–1232. https://doi.org/10.1073/pnas.87.3.1228

King, S.M. 2018. *Dyneins: dynein mechanics, dysfunction, and disease.* Elsevier, Oxford, UK. 530 pp.

King, S.M., T. Otter, and G.B. Witman. 1985. Characterization of monoclonal antibodies against Chlamydomonas flagellar dyneins by high-resolution protein blotting. *Proc. Natl. Acad. Sci. USA.* 82:4717–4721. https://doi.org/10.1073/pnas.82.14.4717

Kubo, T., Y. Hou, D.A. Cochran, G.B. Witman, and T. Oda. 2018. A microtubule-dynein tethering complex regulates the axonemal inner dynein f (I1). *Mol. Biol. Cell.* 29:1060–1074. https://doi.org/10.1091/mbc.E17-11-0689

Lechtreck, K.F., and G.B. Witman. 2007. Chlamydomonas reinhardtii hydin is a central pair protein required for flagellar motility. *J. Cell Biol.* 176:473–482. https://doi.org/10.1083/jcb.200611115

Lechtreck, K.F., P. Delmotte, M.L. Robinson, M.J. Sanderson, and G.B. Witman. 2008. Mutations in Hydin impair ciliary motility in mice. *J. Cell Biol.* 180:633–643. https://doi.org/10.1083/jcb.200710162

Lechtreck, K.F., E.C. Johnson, T. Sakai, D. Cochran, B.A. Ballif, J. Rush, G.J. Pazour, M. Ikebe, and G.B. Witman. 2009. The Chlamydomonas reinhardtii BBSome is an IFT cargo required for export of specific signaling proteins from flagella. *J. Cell Biol.* 187:1117–1132. https://doi.org/10.1083/jcb.200909183

Lechtreck, K.F., T.J. Gould, and G.B. Witman. 2013. Flagellar central pair assembly in Chlamydomonas reinhardtii. *Cilia.* 2:15. https://doi.org/10.1186/2046-2530-2-15

Li, X., R. Zhang, W. Patena, S.S. Gang, S.R. Blum, N. Ivanova, R. Yue, J.M. Robertson, P.A. Lefebvre, S.T. Fitz-Gibbon, et al. 2016. An Indexed, Mapped Mutant Library Enables Reverse Genetics Studies of Biological Processes in Chlamydomonas reinhardtii. *Plant Cell.* 28:367–387. https://doi.org/10.1105/tpc.15.00465

Lin, J., D. Tritschler, K. Song, C.F. Barber, J.S. Cobb, M.E. Porter, and D. Nicastro. 2011. Building blocks of the nexin-dynein regulatory complex in Chlamydomonas flagella. *J. Biol. Chem.* 286:29175–29191. https://doi.org/10.1074/jbc.M111.241760

Loreng, T.D., and E.F. Smith. 2017. The Central Apparatus of Cilia and Eukaryotic Flagella. *Cold Spring Harb. Perspect. Biol.* 9:a028118. https://doi.org/10.1101/cshperspect.a028118

McKenzie, C.W., B. Craige, T.V. Kroeger, R. Finn, T.A. Wyatt, J.H. Sisson, J.A. Pavlik, L. Strittmatter, G.M. Hendricks, G.B. Witman, and L. Lee. 2015. CFAP54 is required for proper ciliary motility and assembly of the central pair apparatus in mice. *Mol. Biol. Cell.* 26:3140–3149. https://doi.org/10.1091/mbc.e15-02-0121

Mitchell, D.R., and M. Nakatsugawa. 2004. Bend propagation drives central pair rotation in Chlamydomonas reinhardtii flagella. *J. Cell Biol.* 166:709–715. https://doi.org/10.1083/jcb.200406148

Mitchell, D.R., and W.S. Sale. 1999. Characterization of a Chlamydomonas insertional mutant that disrupts flagellar central pair microtubule-associated structures. *J. Cell Biol.* 144:293–304. https://doi.org/10.1083/jcb.144.2.293

Mitchell, B.F., L.B. Pedersen, M. Feely, J.L. Rosenbaum, and D.R. Mitchell. 2005. ATP production in Chlamydomonas reinhardtii flagella by glycolytic enzymes. *Mol. Biol. Cell.* 16:4509–4518. https://doi.org/10.1091/mbc.e05-04-0347

Moss, A.G., G.J. Pazour, and G.B. Witman. 1995. Assay of Chlamydomonas phototaxis. *Methods Cell Biol.* 47:281–287. https://doi.org/10.1016/S0091-679X(08)60821-3

Oda, T. 2017. Three-dimensional structural labeling microscopy of cilia and flagella. *Microscopy (Oxf.).* 66:234–244. https://doi.org/10.1093/jmicro/dfx018

Olbrich, H., M. Schmidts, C. Werner, A. Onoufriadis, N.T. Loges, J. Raidt, N.F. Banki, A. Shoemark, T. Burgoyne, S. Al Turki, et al; UK10K Consortium. 2012. Recessive HYDIN mutations cause primary ciliary dyskinesia without randomization of left-right body asymmetry. *Am. J. Hum. Genet.* 91:672–684. https://doi.org/10.1016/j.ajhg.2012.08.016

Pazour, G.J., N. Agrin, J. Leszyk, and G.B. Witman. 2005. Proteomic analysis of a eukaryotic cilium. *J. Cell Biol.* 170:103–113. https://doi.org/10.1083/jcb.200504008

Piperno, G., and D.J. Luck. 1979. Axonemal adenosine triphosphatases from flagella of Chlamydomonas reinhardtii. Purification of two dyneins. *J. Biol. Chem.* 254:3084–3090.

Ponting, C.P. 2006. A novel domain suggests a ciliary function for ASPM, a brain size determining gene. *Bioinformatics.* 22:1031–1035. https://doi.org/10.1093/bioinformatics/btl022

Rao, V.G., R.B. Sarafdar, T.S. Chowdhury, P. Sivadas, P. Yang, P.M. Dongre, and J.S. D'Souza. 2016. Myc-binding protein orthologue interacts with AKAP240 in the central pair apparatus of the Chlamydomonas flagella. *BMC Cell Biol.* 17:24. https://doi.org/10.1186/s12860-016-0103-y

Rompolas, P., R.S. Patel-King, and S.M. King. 2012. Association of Lis1 with outer arm dynein is modulated in response to alterations in flagellar motility. *Mol. Biol. Cell.* 23:3554–3565. https://doi.org/10.1091/mbc.e12-04-0287

Rupp, G., E. O'Toole, and M.E. Porter. 2001. The Chlamydomonas PF6 locus encodes a large alanine/proline-rich polypeptide that is required for assembly of a central pair projection and regulates flagellar motility. *Mol. Biol. Cell.* 12:739–751. https://doi.org/10.1091/mbc.12.3.739

Schou, K.B., S.K. Morthorst, S.T. Christensen, and L.B. Pedersen. 2014. Identification of conserved, centrosome-targeting ASH domains in TRAPPII complex subunits and TRAPPC8. *Cilia.* 3:6. https://doi.org/10.1186/2046-2530-3-6

Schwanhäusser, B., D. Busse, N. Li, G. Dittmar, J. Schuchhardt, J. Wolf, W. Chen, and M. Selbach. 2011. Global quantification of mammalian gene expression control. *Nature.* 473:337–342. https://doi.org/10.1038/nature10098

Shamoto, N., K. Narita, T. Kubo, T. Oda, and S. Takeda. 2018. CFAP70 Is a Novel Axoneme-Binding Protein That Localizes at the Base of the Outer Dynein Arm and Regulates Ciliary Motility. *Cells.* 7:E124. https://doi.org/10.3390/cells7090124

Shapiro, A.J., S.D. Davis, D. Polineni, M. Manion, M. Rosenfeld, S.D. Dell, M.A. Chilvers, T.W. Ferkol, M.A. Zariwala, S.D. Sagel, et al; American Thoracic Society Assembly on Pediatrics. 2018. Diagnosis of Primary Ciliary Dyskinesia. An Official American Thoracic Society Clinical Practice Guideline. *Am. J. Respir. Crit. Care Med.* 197:e24–e39. https://doi.org/10.1164/rccm.201805-0819ST

Shapiro, J., J. Ingram, and K.A. Johnson. 2005. Characterization of a molecular chaperone present in the eukaryotic flagellum. *Eukaryot. Cell.* 4: 1591–1594. https://doi.org/10.1128/EC.4.9.1591-1594.2005

Silflow, C.D., M. LaVoie, L.W. Tam, S. Tousey, M. Sanders, W. Wu, M. Borodovsky, and P.A. Lefebvre. 2001. The Vfl1 Protein in Chlamydomonas localizes in a rotationally asymmetric pattern at the distal ends of the basal bodies. *J. Cell Biol.* 153:63–74. https://doi.org/10.1083/jcb.153.1.63

Silva, J.C., M.V. Gorenstein, G.Z. Li, J.P. Vissers, and S.J. Geromanos. 2006. Absolute quantification of proteins by LCMSE: a virtue of parallel MS acquisition. *Mol. Cell. Proteomics.* 5:144–156. https://doi.org/10.1074/mcp.M500230-MCP200

Smith, E.F., and P.A. Lefebvre. 1996. PF16 encodes a protein with armadillo repeats and localizes to a single microtubule of the central apparatus in Chlamydomonas flagella. *J. Cell Biol.* 132:359–370. https://doi.org/10.1083/jcb.132.3.359

Smith, E.F., and P.A. Lefebvre. 1997. PF20 gene product contains WD repeats and localizes to the intermicrotubule bridges in Chlamydomonas flagella. *Mol. Biol. Cell.* 8:455–467. https://doi.org/10.1091/mbc.8.3.455

Taschner, M., A. Mourão, M. Awasthi, J. Basquin, and E. Lorentzen. 2017. Structural basis of outer dynein arm intraflagellar transport by the transport adaptor protein ODA16 and the intraflagellar transport protein IFT46. *J. Biol. Chem.* 292:7462–7473. https://doi.org/10.1074/jbc.M117.780155

Taylor, B.L., and I.B. Zhulin. 1999. PAS domains: internal sensors of oxygen, redox potential, and light. *Microbiol. Mol. Biol. Rev.* 63:479–506.

Vogt, J.H., and J.H. Schippers. 2015. Setting the PAS, the role of circadian PAS domain proteins during environmental adaptation in plants. *Front. Plant Sci.* 6:513. https://doi.org/10.3389/fpls.2015.00513

Wargo, M.J., E.E. Dymek, and E.F. Smith. 2005. Calmodulin and PF6 are components of a complex that localizes to the C1 microtubule of the flagellar central apparatus. *J. Cell Sci.* 118:4655–4665. https://doi.org/10.1242/jcs.02585

Wirschell, M., D. Nicastro, M.E. Porter, and W.S. Sale. 2009. The regulation of axonemal bending. *In* The Chlamydomonas Sourcebook. Vol. 3: Cell Motility and Behavior. G.B. Witman, editor. Elsevier, New York. 253–282.

Witman, G.B. 1986. Isolation of Chlamydomonas flagella and flagellar axonemes. *Methods Enzymol.* 134:280–290. https://doi.org/10.1016/0076-6879(86)34096-5

Witman, G.B., J. Plummer, and G. Sander. 1978. Chlamydomonas flagellar mutants lacking radial spokes and central tubules. Structure, composition, and function of specific axonemal components. *J. Cell Biol.* 76: 729–747. https://doi.org/10.1083/jcb.76.3.729

Yang, P., L. Fox, R.J. Colbran, and W.S. Sale. 2000. Protein phosphatases PP1 and PP2A are located in distinct positions in the Chlamydomonas flagellar axoneme. *J. Cell Sci.* 113:91–102.

Yang, P., D.R. Diener, J.L. Rosenbaum, and W.S. Sale. 2001. Localization of calmodulin and dynein light chain LC8 in flagellar radial spokes. *J. Cell Biol.* 153:1315–1326. https://doi.org/10.1083/jcb.153.6.1315

Yang, P., D.R. Diener, C. Yang, T. Kohno, G.J. Pazour, J.M. Dienes, N.S. Agrin, S.M. King, W.S. Sale, R. Kamiya, et al. 2006. Radial spoke proteins of Chlamydomonas flagella. *J. Cell Sci.* 119:1165–1174. https://doi.org/10.1242/jcs.02811

Yokoyama, R., E. O'toole, S. Ghosh, and D.R. Mitchell. 2004. Regulation of flagellar dynein activity by a central pair kinesin. *Proc. Natl. Acad. Sci. USA.* 101:17398–17403. https://doi.org/10.1073/pnas.0406817101

Zhang, H., and D.R. Mitchell. 2004. Cpc1, a Chlamydomonas central pair protein with an adenylate kinase domain. *J. Cell Sci.* 117:4179–4188. https://doi.org/10.1242/jcs.01297

Zhang, Z., I. Kostetskii, W. Tang, L. Haig-Ladewig, R. Sapiro, Z. Wei, A.M. Patel, J. Bennett, G.L. Gerton, S.B. Moss, et al. 2006. Deficiency of SPAG16L causes male infertility associated with impaired sperm motility. *Biol. Reprod.* 74:751–759. https://doi.org/10.1095/biolreprod.105.049254

Zhang, Z., W. Tang, R. Zhou, X. Shen, Z. Wei, A.M. Patel, J.T. Povlishock, J. Bennett, and J.F. Strauss III. 2007. Accelerated mortality from hydrocephalus and pneumonia in mice with a combined deficiency of SPAG6 and SPAG16L reveals a functional interrelationship between the two central apparatus proteins. *Cell Motil. Cytoskeleton.* 64:360–376. https://doi.org/10.1002/cm.20189